Electronic supplementary materials *Mendeleev Commun.*, 2022, **32**, 367–370

Optical and electrochemical properties of novel fused tricyclic thiophene–15-crown-5 systems and their complexes with Mg and Ba ions

Sergey D. Tokarev, Anatoly Botezatu, Andrey V. Khoroshutin, Yury V. Fedorov and Olga A. Fedorova

Table of contents

Experimental Section

All reagents were purchased from Acros, Aldrich, Merck and used without additional purification. Solvents were purified by standard procedures. Spectroscopic grade MeCN, was used for spectroscopic and fluorometric measurements.

^{1}H and ^{13}C (APT method) NMR spectra were recorded on a Bruker AVANCE-400 and INOVA-400 spectrometers. The chemical shifts and spin-spin coupling constants were determined with accuracy of 0.01 ppm and 0.1 Hz, respectively. Flash column chromatography was carried out at Biotage Isolera Prime chromatograph. Aluminum oxide was hand-packed into the cartridge using the wet method. Elemental analysis was performed in the A. N. Nesmeyanov Institute of Organoelement Compounds of Russian Academy of Sciences.

ESI mass spectra (ESI-MS) were acquired on a Finnigan LCQ Advantage tandem dynamic mass spectrometer (USA) equipped with a mass analyzer with an octapole ionic trap, a MS Surveyor pump, a Surveyor autosampler, a Schmidlin-Lab nitrogen generator (Germany), and a system of data collection and processing using the X Calibur program, version 1.3 (Finnigan). The mass spectra were measured in the positive ion mode. Samples in MeCN were injected directly into the source at flow rate 50 μL min-1 through a Reodyne injector with a loop of 20 μL. The temperature of the transfer capillary was 150°C, and the electrospray needle was held at potential 4.0 kV.

UV-Vis spectra were recorded on Cary 300 spectrometer, for the fluorescence spectra Cary Eclipse spectrofluorometer has been used. UV-Vis titration have been performed as follows. To a solution of a ligand portion ($2 \cdot 10^{-5}$ M, 2.5 ml), solutions of $Mg(ClO_4)_2$ or $Ba(ClO_4)_2$ (10^{-3} M) have been added successively to maintain a noticeable changes in a spectrum of the resulting solution. The titration was ended when there was no noticeable change of the spectrum upon the addition of the next portion of the titration solution.

All measured luminescence spectra were corrected for non-uniformity of detector spectral sensitivity. Quinine bisulfate in 1N H_2SO_4 (φ_{fl} = 0,546) was used as reference for the luminescence quantum yield measurements. The luminescence quantum yields were calculated using equation:

$$\varphi_i = \varphi_0 \frac{(1 - 10^{-A_0}) * S_i * {n_i}^2}{(1 - 10^{-A_i}) * S_0 * {n_0}^{2'}}$$

where φ_i and φ_0 are the luminescence quantum yields of the studied solution and the standard compound, respectively; A_i and A_0 are the absorptions of the studied solution and the standard, respectively; S_i and S_0 are the areas underneath the curves of the luminescence spectra of the studied solution and the standard, respectively; and n_i and n_0 are the refractive indices of the solvents for the substance under study and the standard compound (n_i = 1.3288, acetonitrile; n_0 = 1.3391, 1 N H_2SO_4)

Electrochemical measurements were carried out at 22 °C with a Metrohm Autolab B.V. potentiostate. Cyclic voltammetry experiments were performed in three-electrode cell equipped with a glassy carbon (GC) electrode (disk, d = 2 mm), Ag/AgCl/KCl (aq. saturated; reference electrode), and platinum electrode (counter electrode). Compounds were dissolved in degassed dry MeCN containing Bu_4NPF_6 as the supporting electrolyte (0.1 M). Dry argon gas was bubbled through the solutions for 30 min before cyclic voltammetry experiments. The scan rate was 200 mV s^{-1}. Ferrocene/ferrocenium pair was used as internal standard for all voltammetry experiments (0.414 V relative to the reference electrode used). Spectroelectrochemistry measurements were carried out with the same potentiostat, Honeycomb Spectroelectrochemistry Cell Kit and Avantes AvaSpec-2048 spectrophotometer.

Synthesis of ligands

*(E)-15-(2-(Thiophen-3-yl)vinyl)-2,3,5,6,8,9,11,12-octahydrobenzo[b][1,4,7,10,13]pentaoxacyclopentadecine (**3a**).*

Phosphonate **1a** (240 mg, 0.96 mmol) and NaH (60% dispersion in mineral oil, 120 mg, 3 mmol) were dissolved in DME (10 ml) and stirred for 30 min. Next, aldehyde **2** (300 mg, 0.96 mmol) was added. The mixture was stirred for 4 h at 40 °C and then overnight at room temperature. The solution was then poured into water-ice mixture, the precipitate formed was filtered and recrystallized from methanol (15 ml). Yield: 230 mg (64%). ^{1}H NMR ($CDCl_3$) δ_H ppm, J/Hz: 3.78 (8H, s), 3.94 (4H, m), 4.16 (2H, m), 4.20 (2H, m), 6.85 (1H, d, J=15.8), 6.85 (1H, s), 6.99-7.01 (2H, m, Th-), 7.02-7.04(2H, m), 7.09 (1H, d, J=16.0), 7.17 (1H, d, J=5.1).

*(E)-15-(2-(Thiophen-2-yl)vinyl)-2,3,5,6,8,9,11,12-octahydrobenzo[b][1,4,7,10,13]pentaoxacyclopentadecine (**3b**).*

The same procedure as for **3a** using phosphonate **1b** (240 mg, 0.96 mmol), NaH (120 mg, 60% in mineral oil, 3 mmol), aldehyde **3** (300 mg, 0.96 mmol) and DME (5 ml). Yield 226 mg (62%). ^{1}H NMR ($CDCl_3$) δ_H ppm, J/Hz: 3.78 (8H, s), 3.94 (4H, m), 4.16 (2H, m), 4.21 (2H, m), 6.85 (1H, d, J=8.1), 6.88 (1H, d, J=16.1), 6.99 (1H, d, J=15.8), 7.01 (1H, dd J = 8.2, 1.8), 7.04 (1H, d J = 1.8), 7.23 (1H, m), 7.32 (2H, m).

Photocyclization procedure. All photocyclization reactions were carried out in a photoreactor, containing a water-cooled quartz well, immersed into the cylinder-shaped flask equipped with a reflux condenser and an argon inlet. The well is thermostated with a water run external thermostat. In a typical experiment, a solution of stilbene (50 mg) in benzene (100 ml), iodine (1.25 equiv.) and propylene oxide (1000 equiv.) have been placed to a photoreactor. The reaction mixture was irradiated with the light of a submerged mercury lamp at 45 °C for 2 h in the stream of argon. Color of iodine has disappeared, and the reaction mixture has been evaporated. The combined residues of three 50 mg runs were chromatographed on SiO_2, eluent EtOAc-dioxane.

*8,9,11,12,14,15,17,18-Octahydrothieno[2',3':5,6]naphtho[2,3-b][1,4,7,10,13]-pentaoxacyclopentadecine (**4a**).*

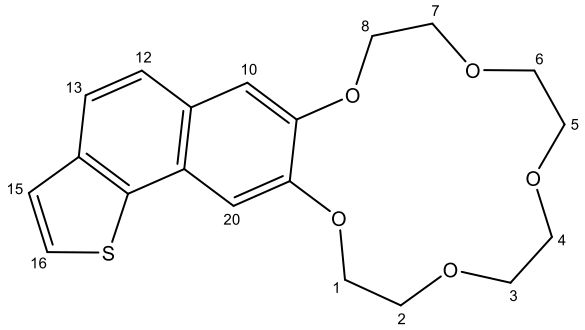

Yield: 24 %. ^{1}H NMR (CD_3CN) δ_H ppm, J/Hz: 3.67 (4H, m, $H_{4,5}$), 3.71 (4H, m, $H_{3,6}$), 3.90 (4H, m, $H_{2,7}$), 4.23 (2H, m, H_8), 4.28 (2H, m, H_1), 7.39 (1H, s, H_{20}), 7.41 (1H, s, H_{10}), 7.49 (1H, d, J=5.3, H_{15}), 7.57 (1H, d, J=5.3, H_{16}), 7.67 (1H, d, J=8.5, H_{12}), 7.76 (1H, d, J=8.6, H_{13}). ^{13}C NMR (CD_3CN, δ_H ppm., J/Hz): 67.69 (1C-8), 67.73 (1C-1), 67.96 (1C-7),68.03 (1C-2),68.70-68.71 (2C-4,5), 69.51-69.52 (2C-3,6), 104.71 (1C-10), 109.92 (1C-20), 120.67(1C-13), 124.17 (1C-12), 128.87 (1C-15), 125.30 (1C-16). Signals of quaternary ^{13}C could not be accumulated due to the low solubility of the substance. MS (ESI), m/z: 374.12 $[M]^+$ (100 %). Calc. for $C_{20}H_{22}O_5S$ (%): C, 64.15; H, 5.92, S, 8.56 found (%): C, 64.19; H, 5.97; S, 8.61.

*2,3,5,6,8,9,11,12-Octahydrothieno[3',2':7,8]naphtho[1,2-b][1,4,7,10,13]-pentaoxacyclopentadecine (**4'a**).*

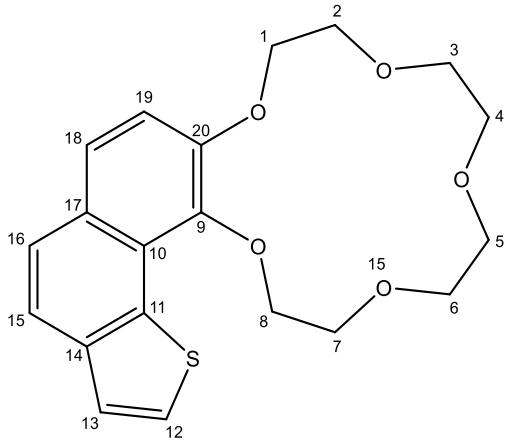

Yield: 36 %. ^{1}H NMR (CD_3CN) δ_H ppm, J/Hz: 3.68 (6H, m,H $_{4,5,6}$), 3.76 (2H, m, H_3), 3.91 (2H, m, H_7), 4.17 (2H, tr, J= 5.3, H_2),), 4.31 (m, 2H, H_8), 4.40 (m, 2H, H_1), 7.38 (1H, d, J= 8.9, H_{19}), 7.52 (1H, d, J=5.4, H_{13}), 7.69 (1H, d, J=5.4, H_{12}), 7.73 (1H, d, J=8.3, H_{18}), 7.76 (1H, d, J=8.9, H_{13}), 7.77 (1H, d, J=8.7, H_{12}). ^{13}C NMR (CD_3CN, δ_H ppm., J/Hz):68.70 (1C-8), 69.09 (1C-7), 69.79 (2C-3,4), 70.05 (1C-2), 70.34, 70.62 (2C-5,6), 72.37 (1C-1), 113.96 (1C-19), 120.46 (1C-15), 124.00 (1C-13), 124.55 (1C-16), 124.87 (1C-18), 127.78 (1C-12). Signals of quaternary ^{13}C could not be accumulated due to the low solubility of the substance. MS (ESI), m/z: 374.09 $[M]^+$ (100 %). Calc. for C20H22O5S (%): C, 64.15; H, 5.92, S, 8.56 found (%): C, 64.23; H, 5.99; S, 8.62.

*8,9,11,12,14,15,17,18-Octahydrothieno[3',2':5,6]naphtho[2,3-b][1,4,7,10,13]-pentaoxacyclopentadecine (**4b**).*

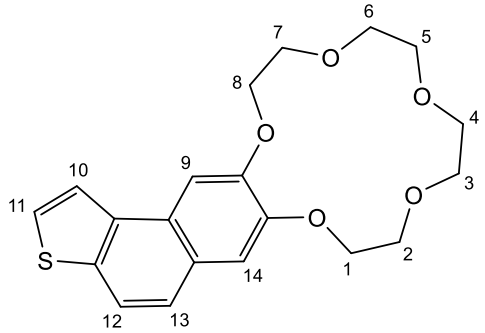

Yield: 42%. ^{1}H NMR (CD_3CN) δ_H ppm, J/Hz: 3.66 (4H, m, $H_{4,5}$), 3.70 (4H, m, $H_{3,6}$), 3.89 (4H, m, $H_{2,7}$), 4.21 (2H, m, H_8), 4.29 (2H, m, H_1), 7.37 (1H, s, H_9), 7.41 (1H, s, H_{10}), 7.65-7.68 (2H, m, $H_{10,13}$), 7.73 (1H, s, H_{14}), 7.82 (1H, dd, J=8.7, J=0.7 H_{12}), 8.00 (1H, dd, J=5.5, J=0.8 H_{11}). ^{13}C NMR (CD_3CN, δ_H ppm.): 67.87, 68.04, 68.46, 69.35, 70,23, 104.64, 108.84, 118.26, 121.63, 123.49, 125.46. MS (ESI), m/z: 374.12 $[M]^+$ (100 %). Calc. for $C_{20}H_{22}O_5S$ (%): C, 64.15; H, 5.92, S, 8.56 found (%): C, 64.17, H, 5.95; S, 8.58.

*2,3,5,6,8,9,11,12-Octahydrothieno[2',3':7,8]naphtho[1,2-b][1,4,7,10,13]-pentaoxacyclopentadecine (**4'b**).*

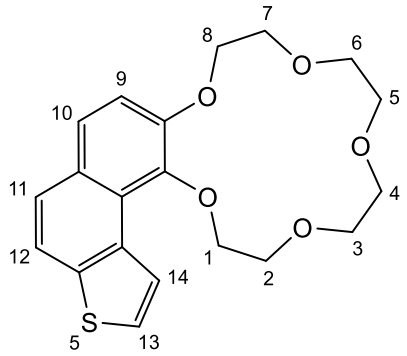

Yield: 20 %. ^{1}H NMR (CD_3CN) δ_H ppm, J/Hz: 3.67-3.70 (6H, m, H $_{4,5,6}$), 3.75 (2H, m, H_3), 3.91 (2H, m, H_7), 4.11 (2H, tr, J= 5.6, H_2), 4.28 (m, 4H, $H_{1,8}$), 7.39 (1H, d, J= 8.9, H_9), 7.69 (1H, dd, J=5.5, J=0.5 H_{14}), 7.72 (1H, d, J=8.7, H_{11}), 7.75 (1H, d, J=8.9, H_{10}), 7.83 (1H, dd, J=0.7, J=8.7 H_{13}). ^{13}C NMR (CD_3CN, δ_H ppm.): 68.21, 68.69, 69.25, 69.30, 69.53, 69.74, 70.25, 71.80, 113.64, 124.39, 124.66, 124.74, 126.06, 127.03. MS (ESI), m/z: 374.11 $[M]^+$ (100 %). Calc. for $C_{20}H_{22}O_5S$ (%): C, 64.15; H, 5.92, S, 8.56 found (%): C, 64.13; H, 5.91; S, 8.53.

NMR spectra

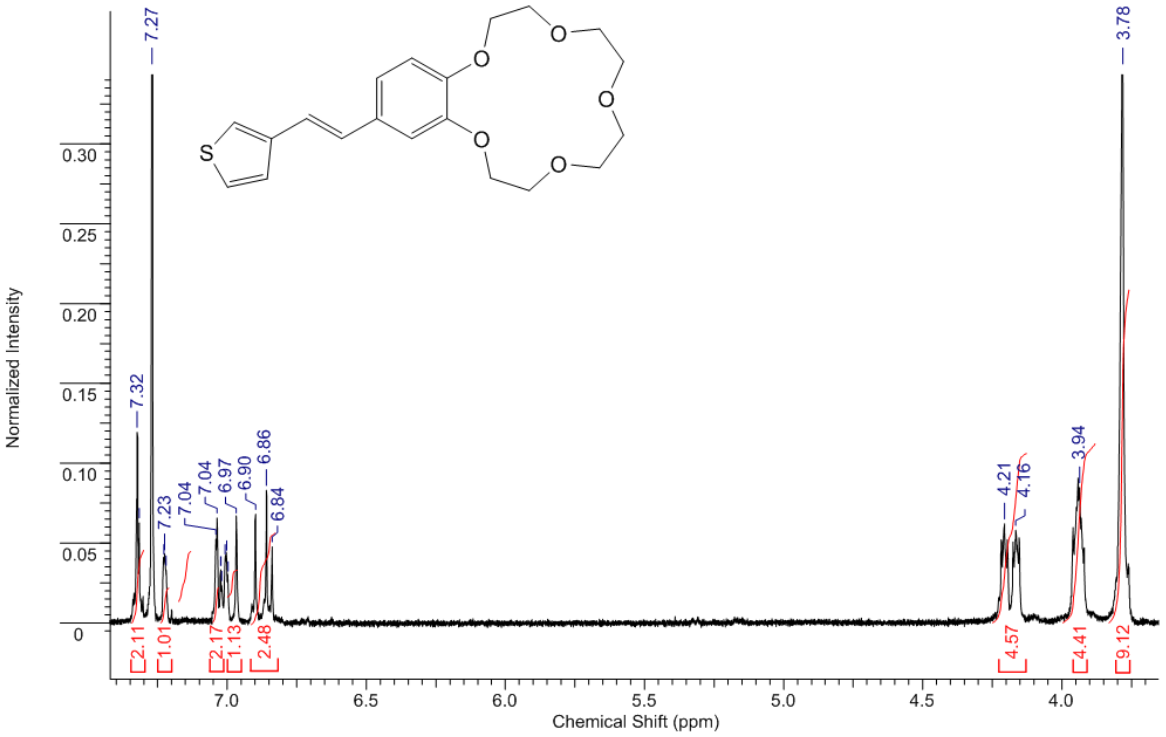

Figure S1. ^{1}H NMR spectrum of the **3a** in $CDCl_3$ solution

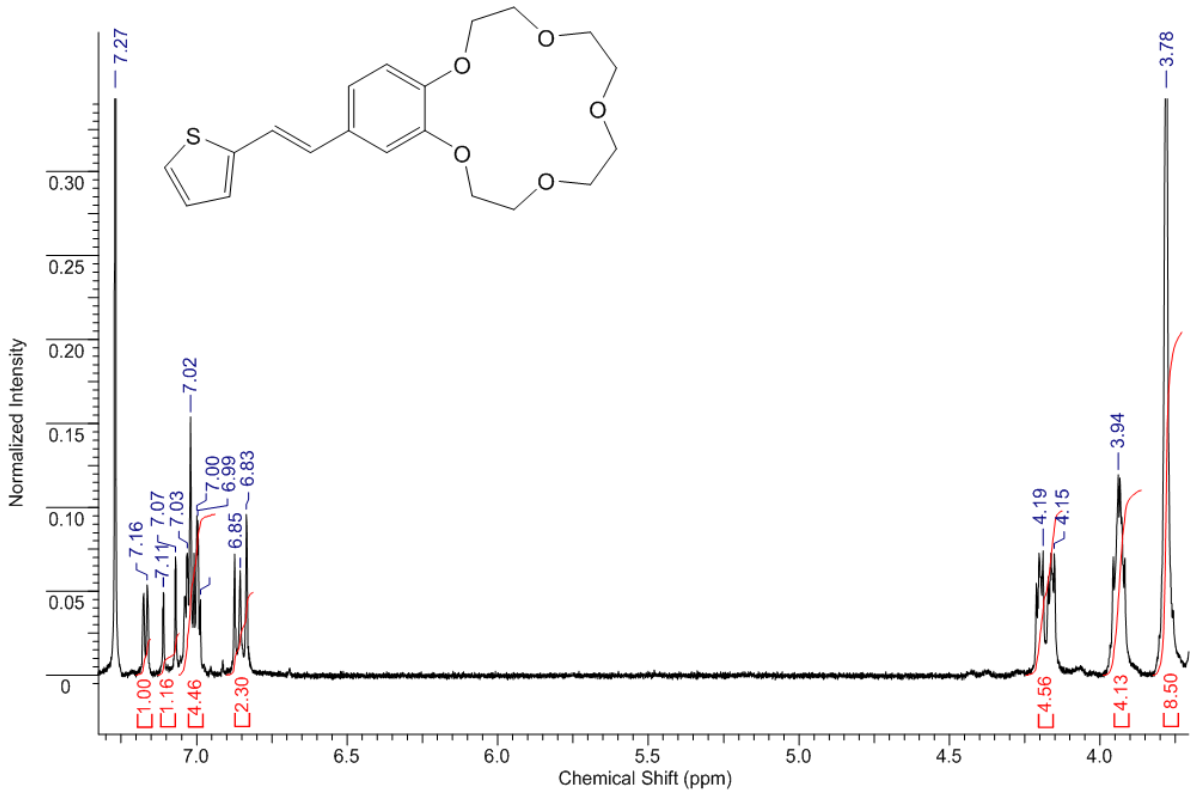

Figure S2. ^{1}H NMR spectrum of the **3b** in $CDCl_3$ solution

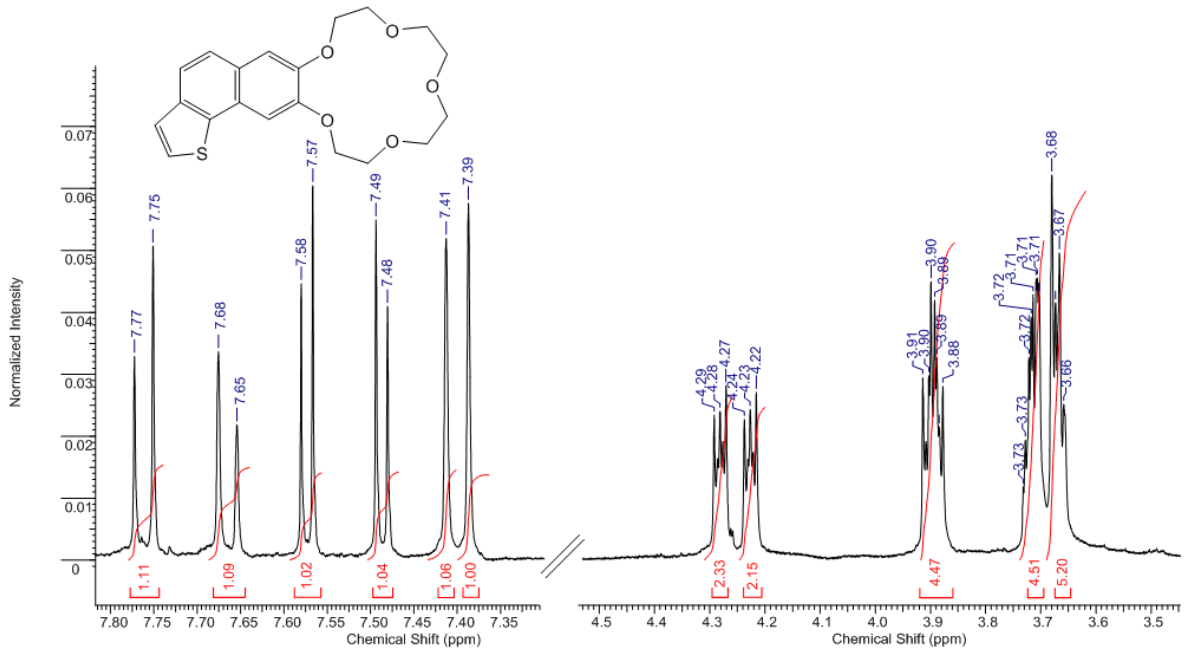

Figure S3. ^{1}H NMR spectrum of the **4a** in CD_3CN-d_3 solution

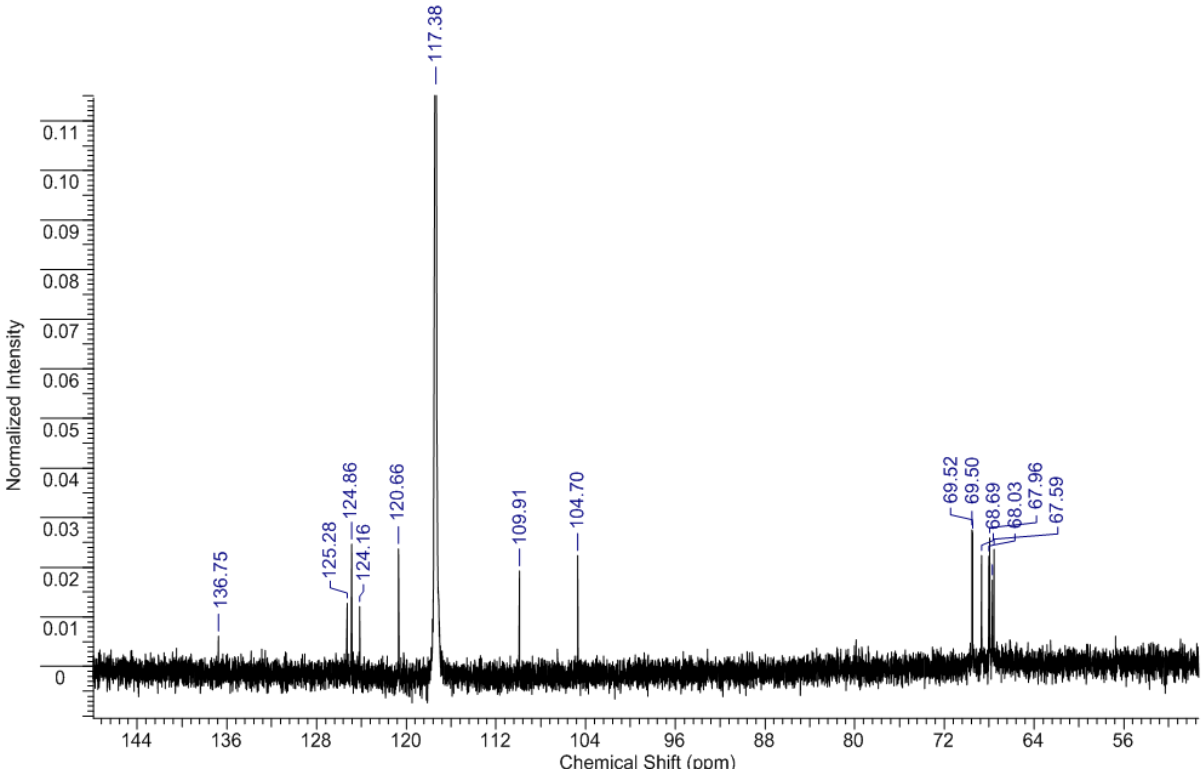

Figure S4. ^{13}C NMR spectrum of the **4a** in CD_3CN-d_3 solution

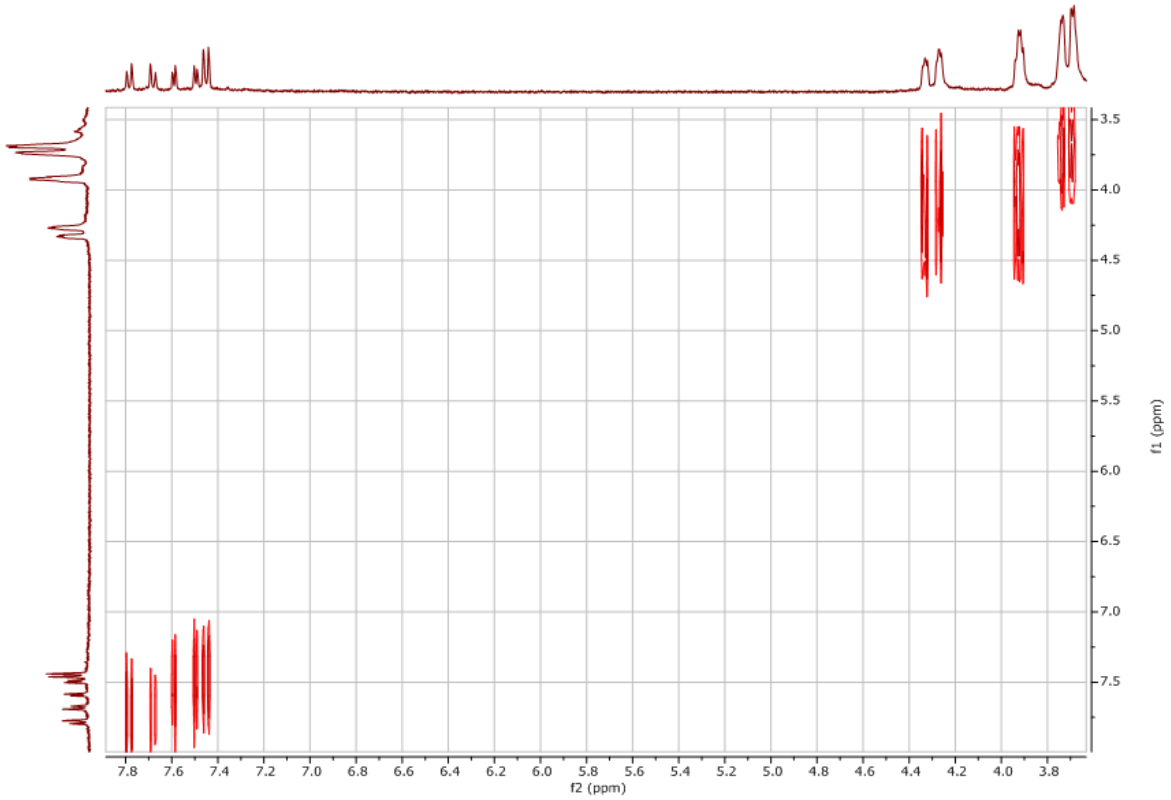

Figure S5. COSY ^{1}H-^{1}H NMR spectrum of the **4a** in CD_3CN-d_3 solution

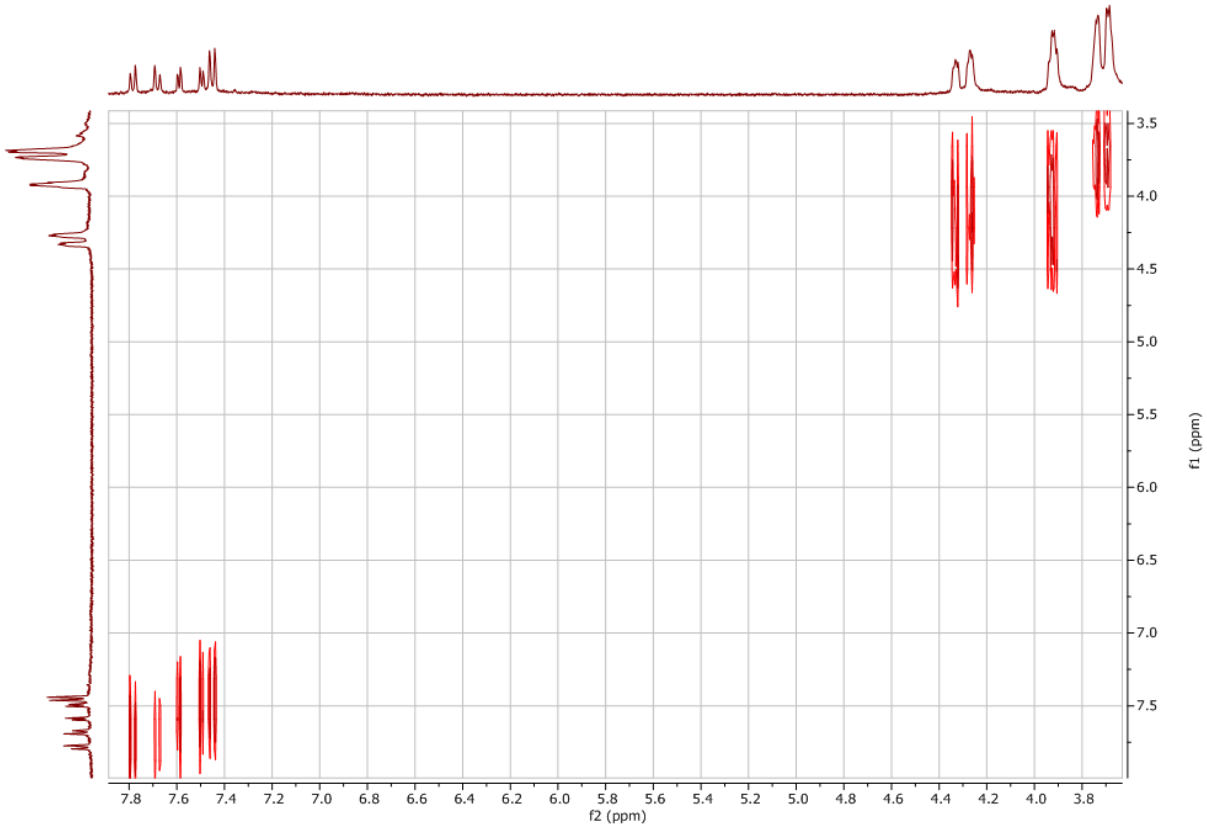

Figure S6. HMBC ^{1}H-^{13}C NMR spectrum of the **4a** in CD_3CN-d_3 solution

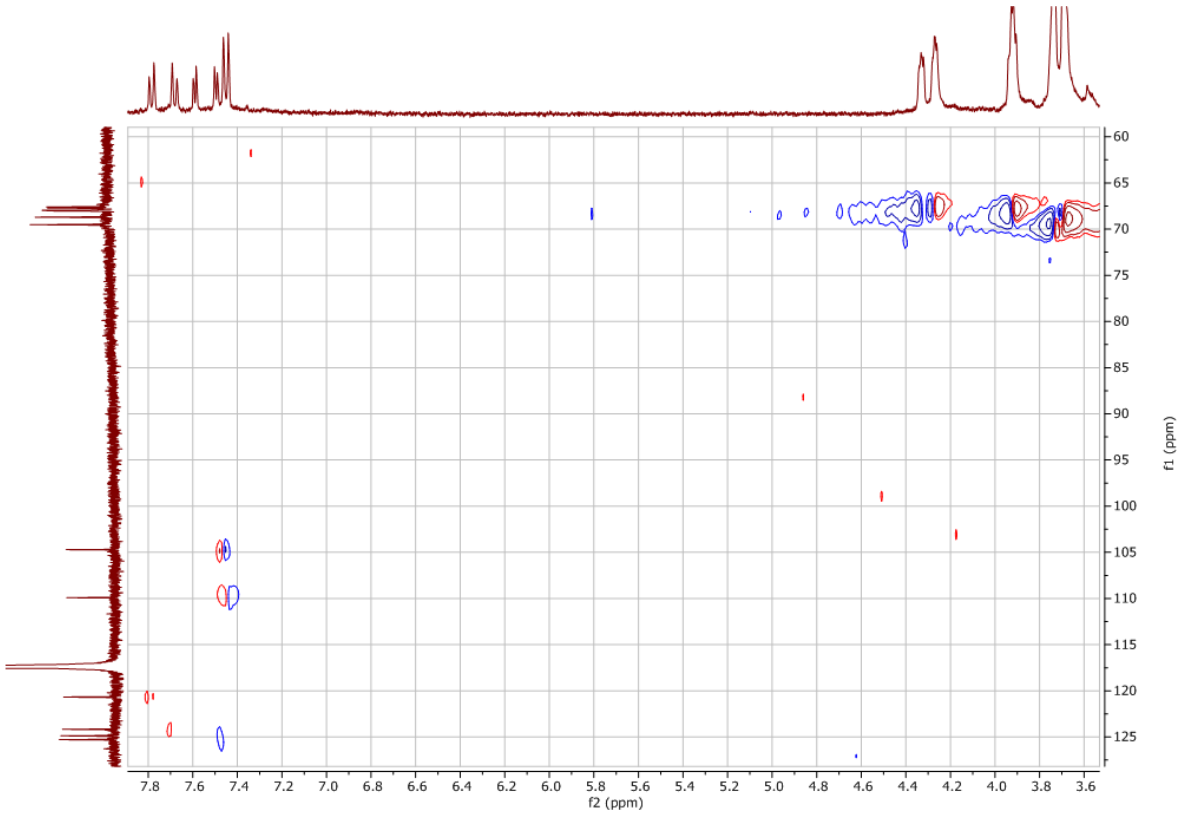

Figure S7. HSQC ^{1}H-^{13}C NMR spectrum of the **4a** in CD_3CN-d_3 solution

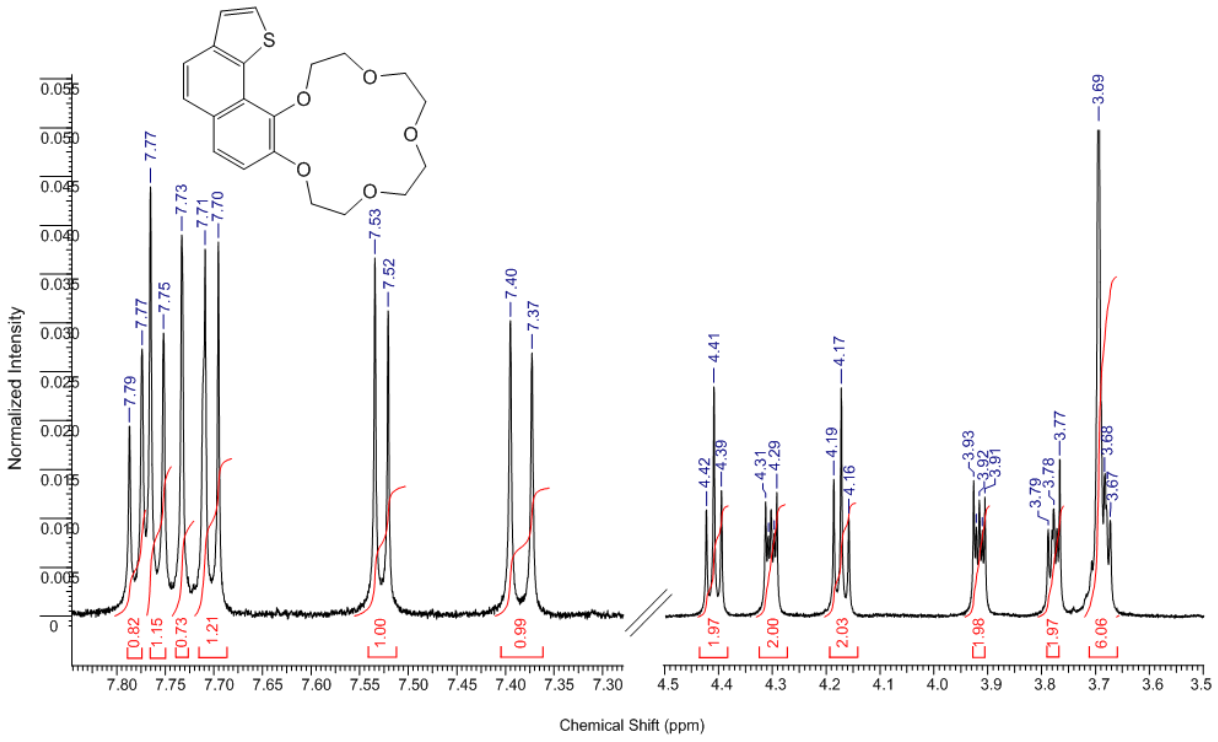

Figure S8. ^{1}H NMR spectrum of the **4'a** in CD_3CN-d_3 solution

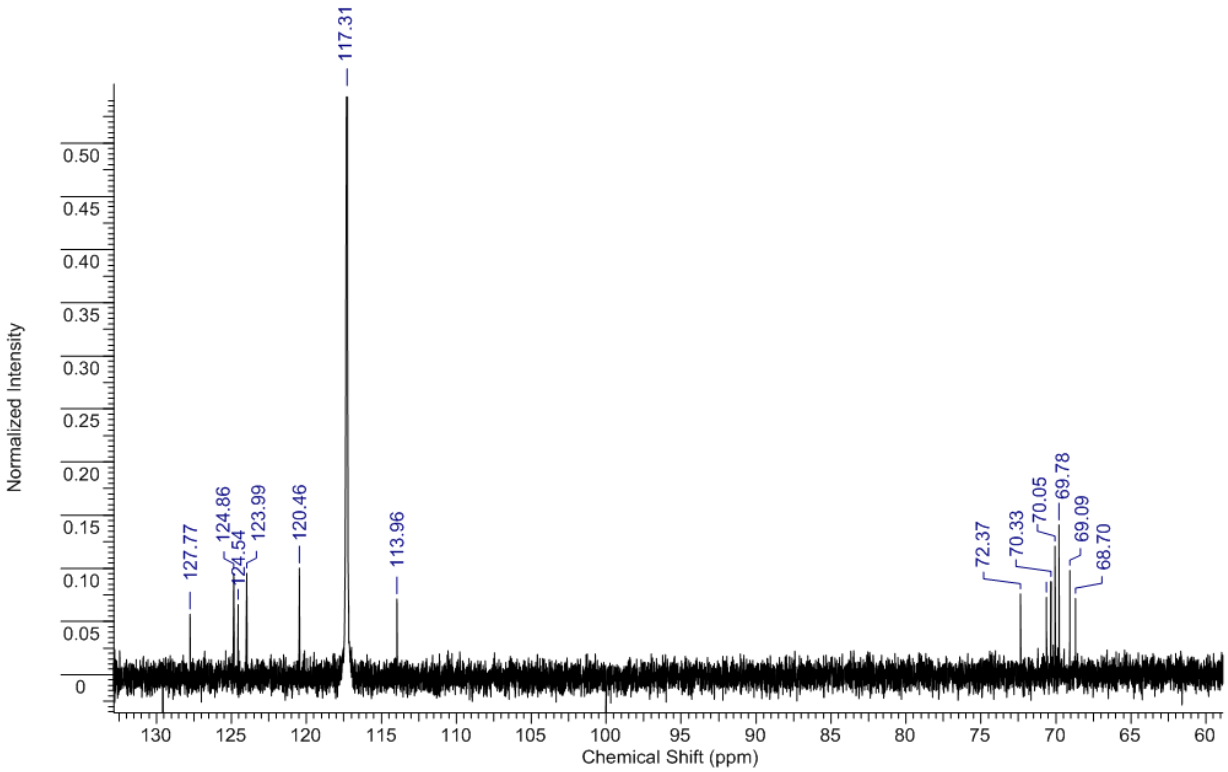

Figure S9. ^{13}C NMR spectrum of the **4'a** in CD_3CN-d_3 solution

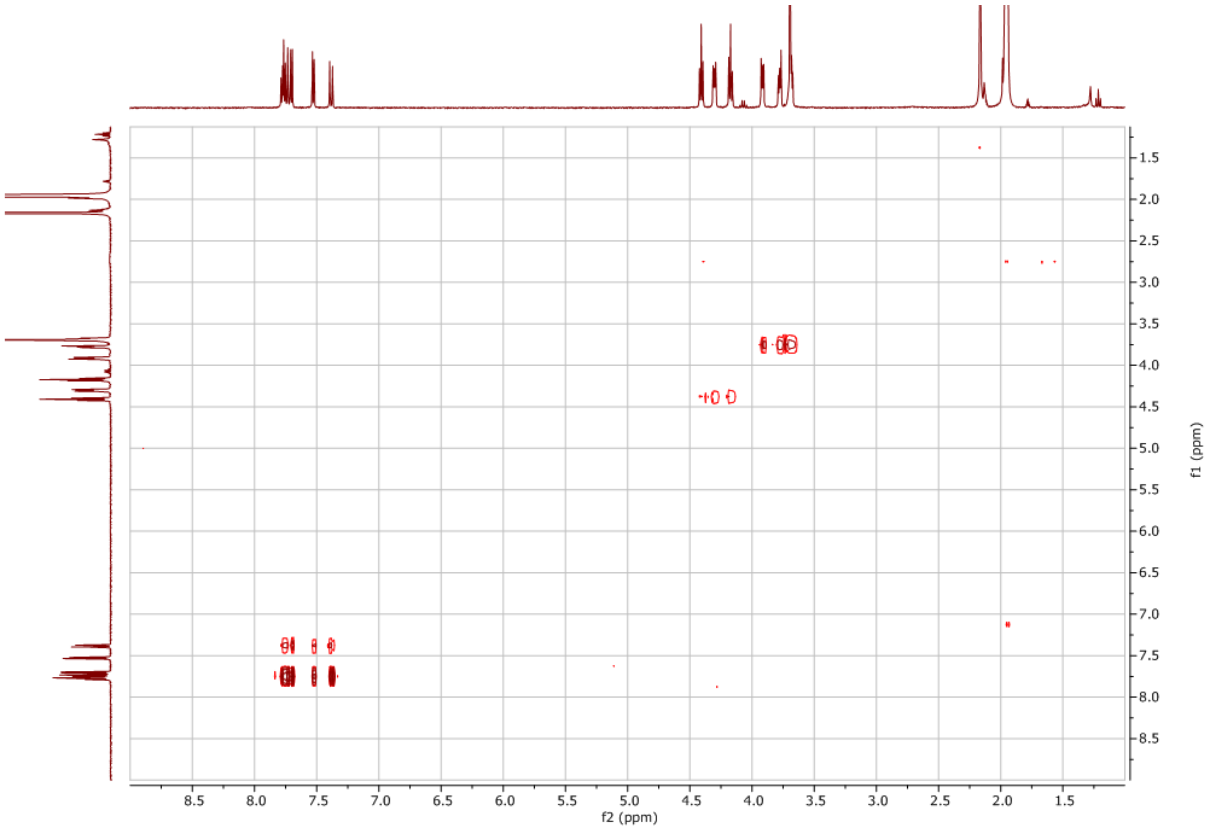

Figure S10. COSY ^{1}H-^{1}H NMR spectrum of the **4'a** in CD_3CN-d_3 solution

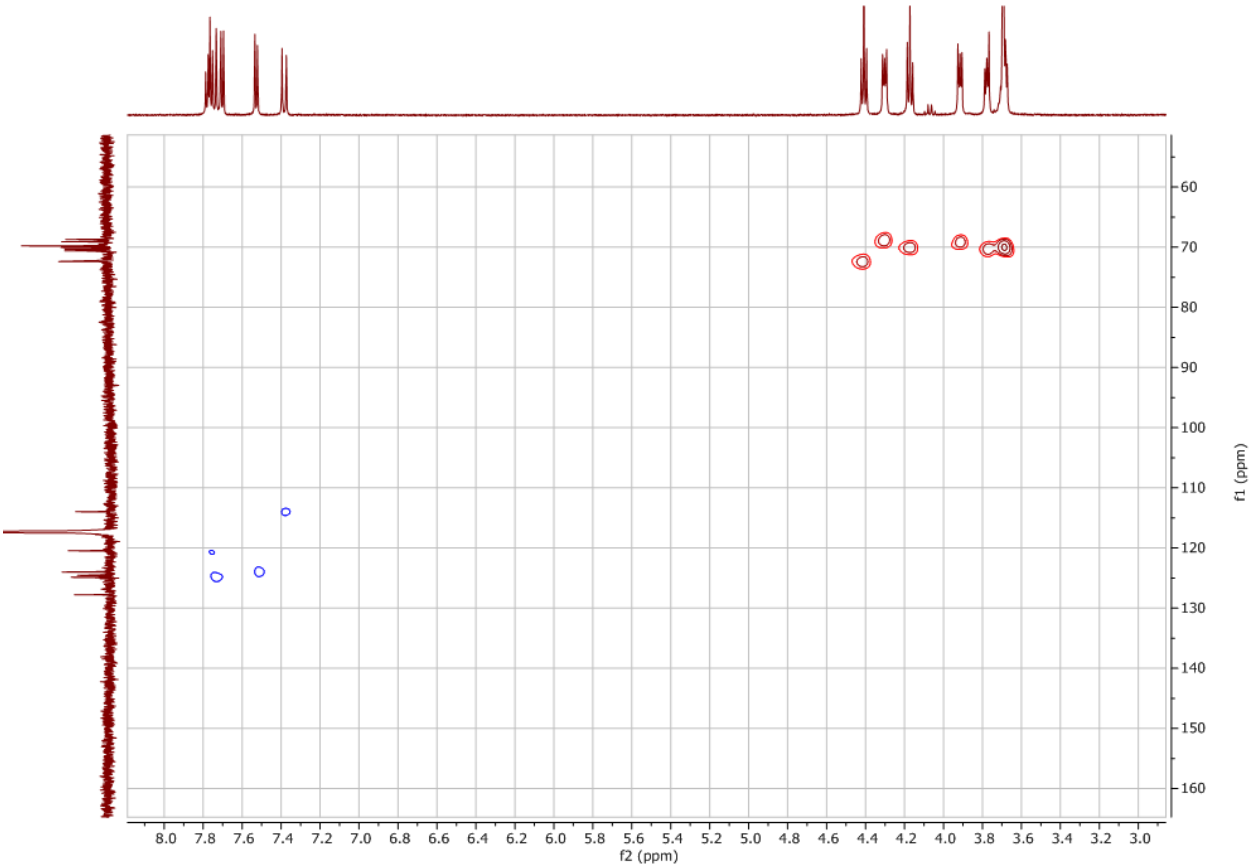

Figure S11. HSQC ^{1}H-^{13}C NMR spectrum of the **4'a** in CD_3CN-d_3 solution

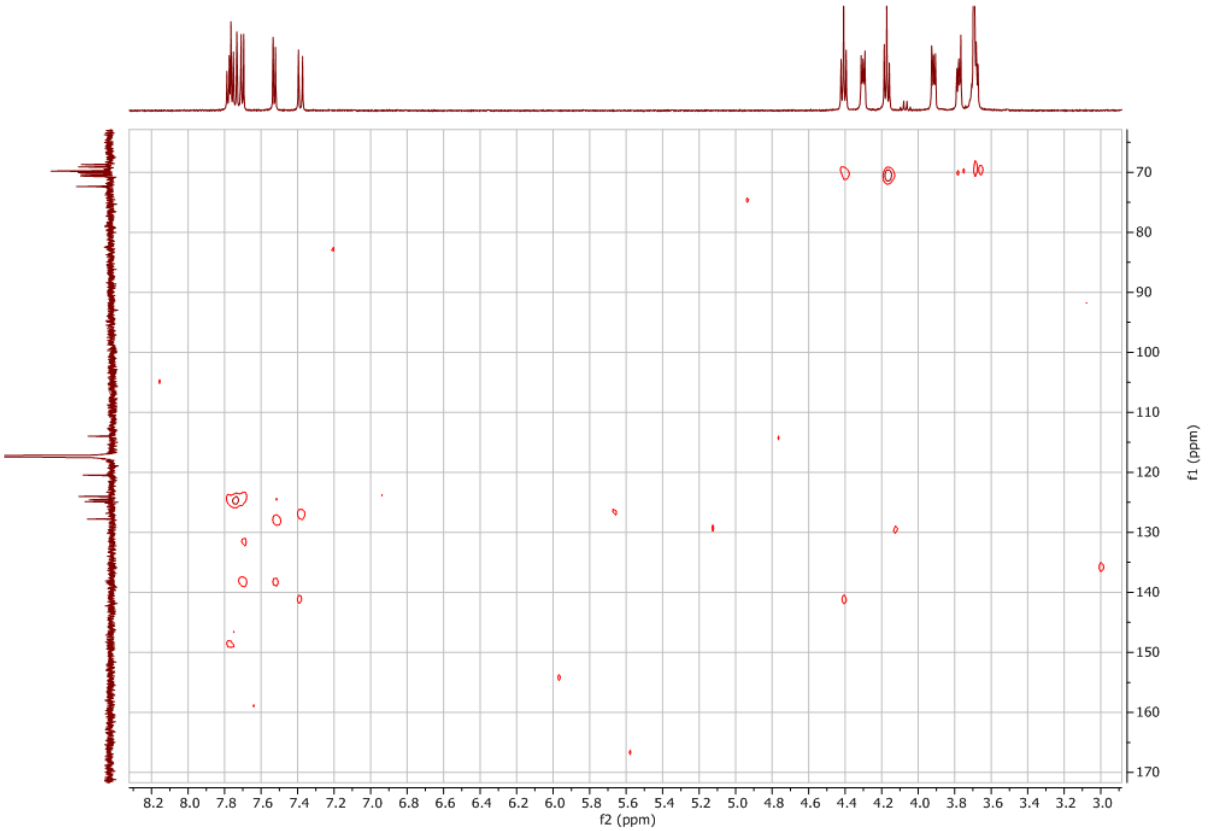

Figure S12. HMBC ^{1}H-^{13}C NMR spectrum of the **4'a** in CD_3CN-d_3 solution

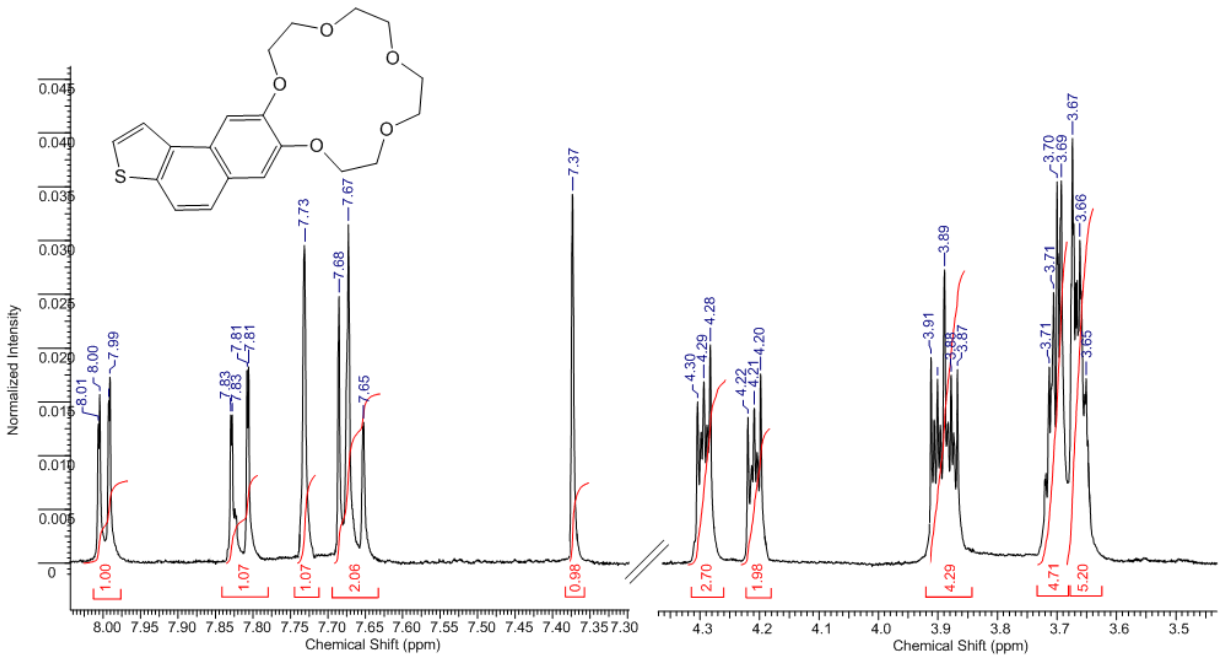

Figure S13. ^{1}H NMR spectrum of the **4b** in CD_3CN-d_3 solution

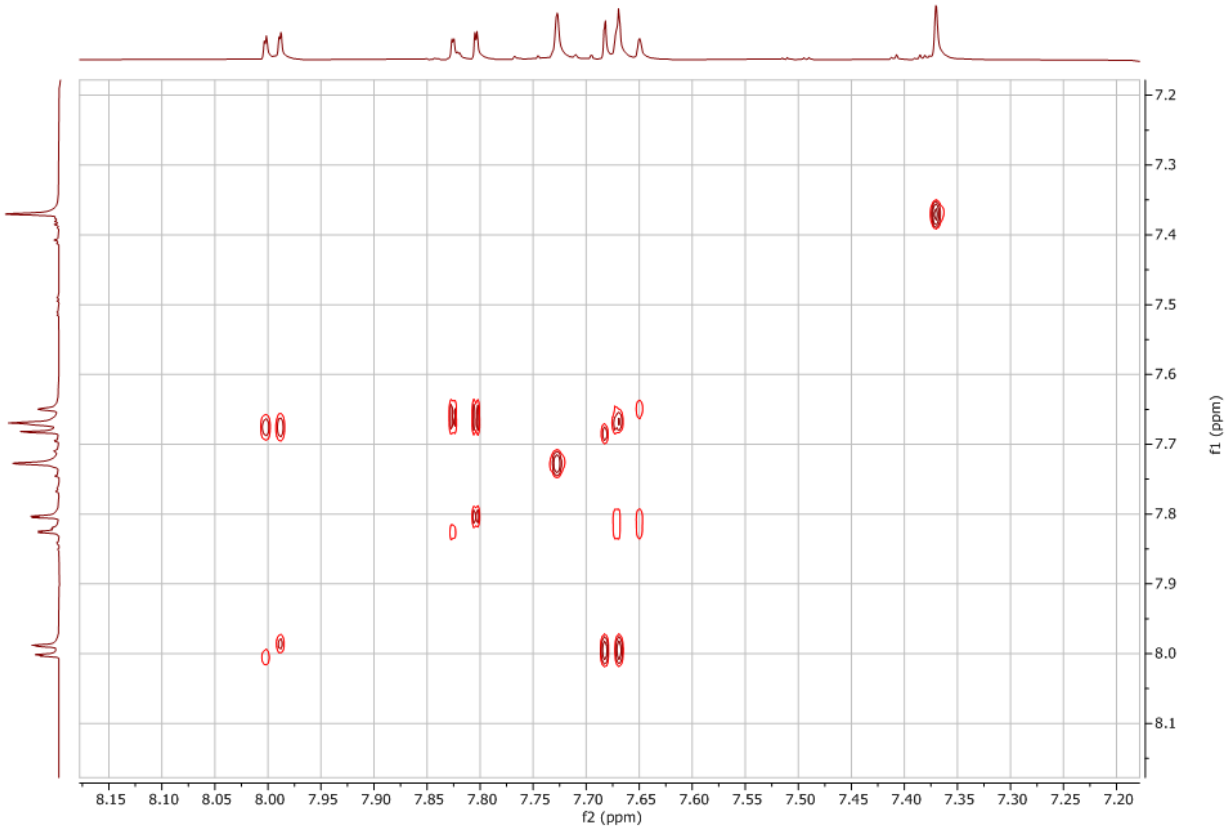

Figure S14. COSY ^{1}H-^{1}H NMR (aromatic part) spectrum of the **4b** in CD_3CN-d_3 solution

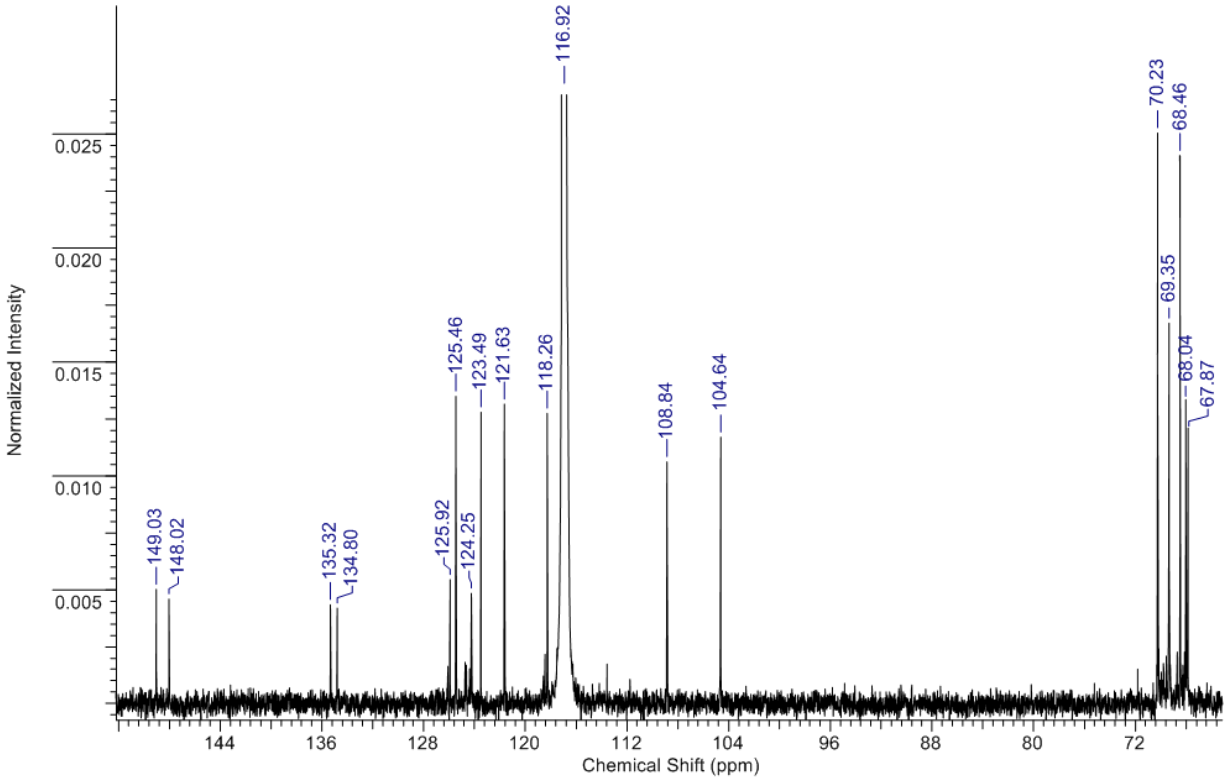

Figure S15. ^{13}C NMR spectrum of the **4b** in CD_3CN-d_3 solution

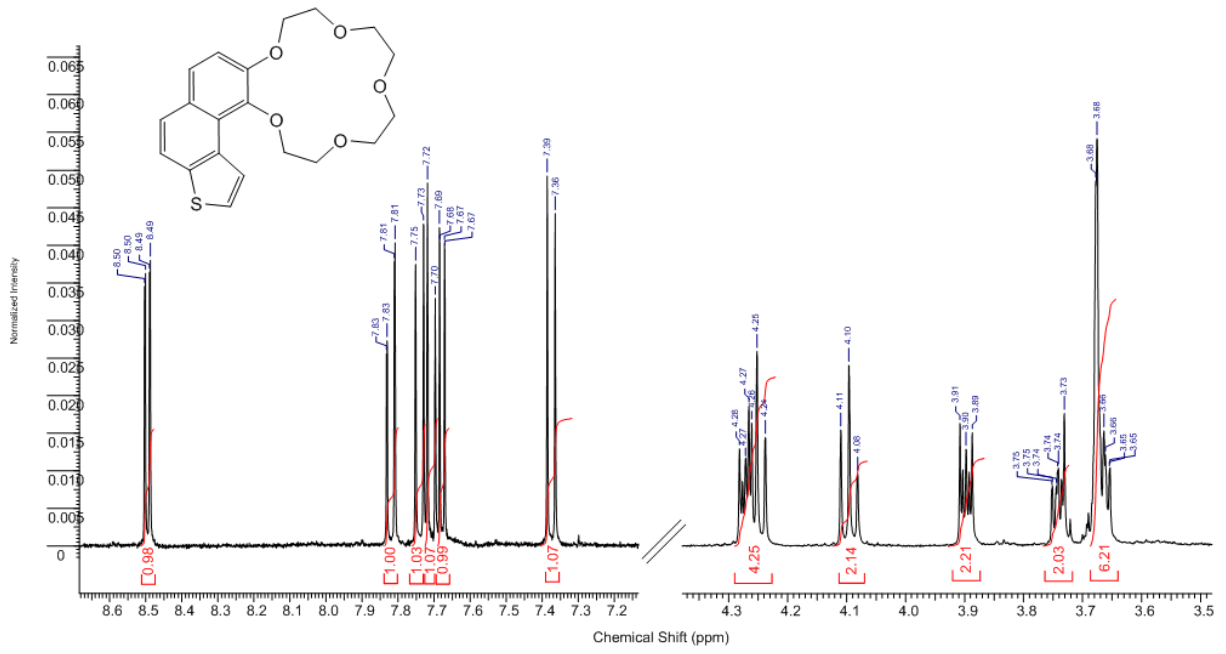

Figure S16. ^{1}H NMR spectrum of the **4'b** in CD_3CN-d_3 solution

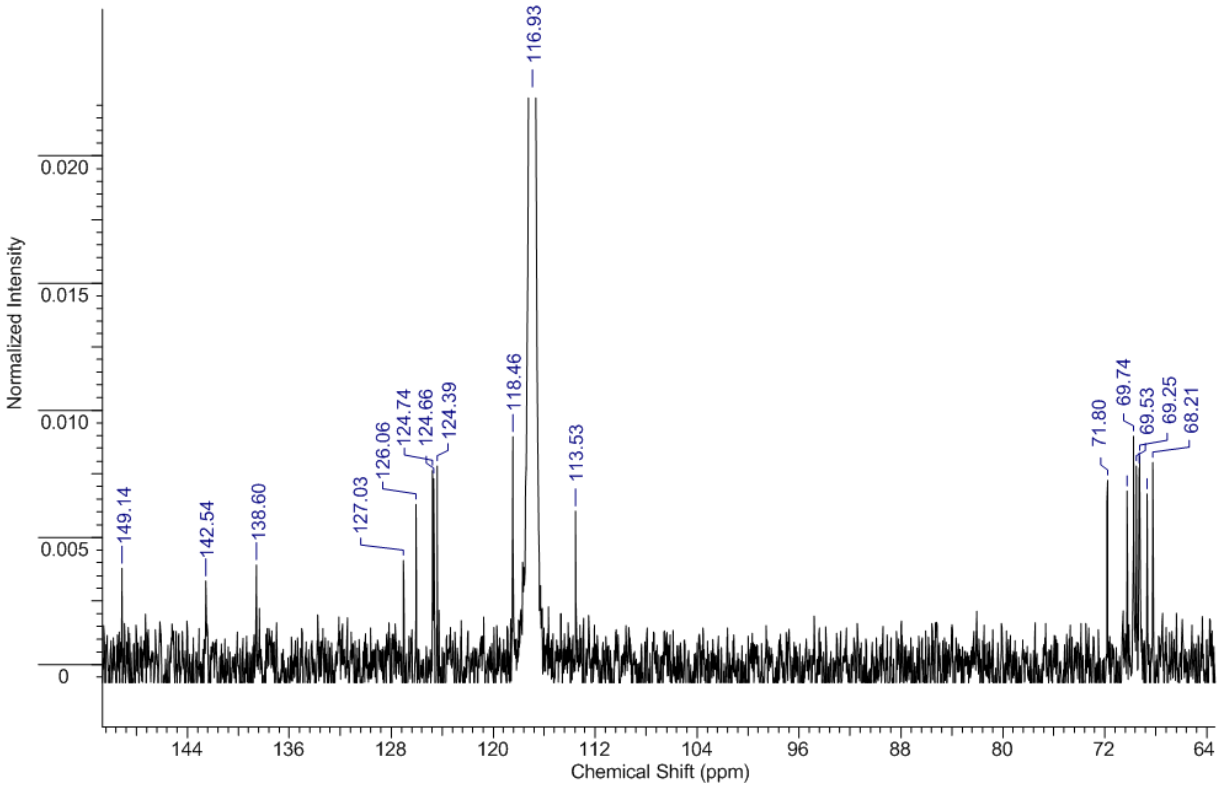

Figure S17. ^{13}C NMR spectrum of the **4'b** in CD_3CN-d_3 solution

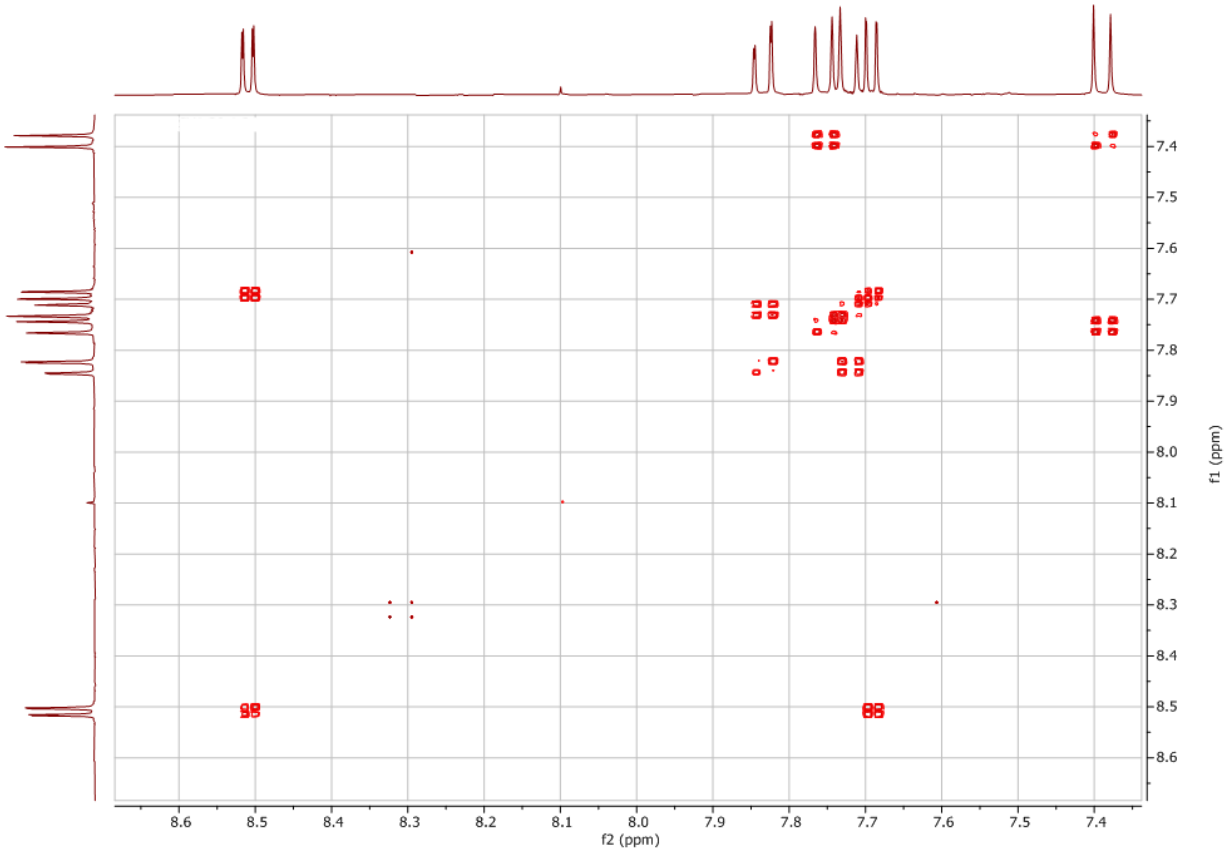

Figure S18. COSY ^{1}H-^{1}H NMR spectrum of the **4'b** in CD_3CN-d_3 solution

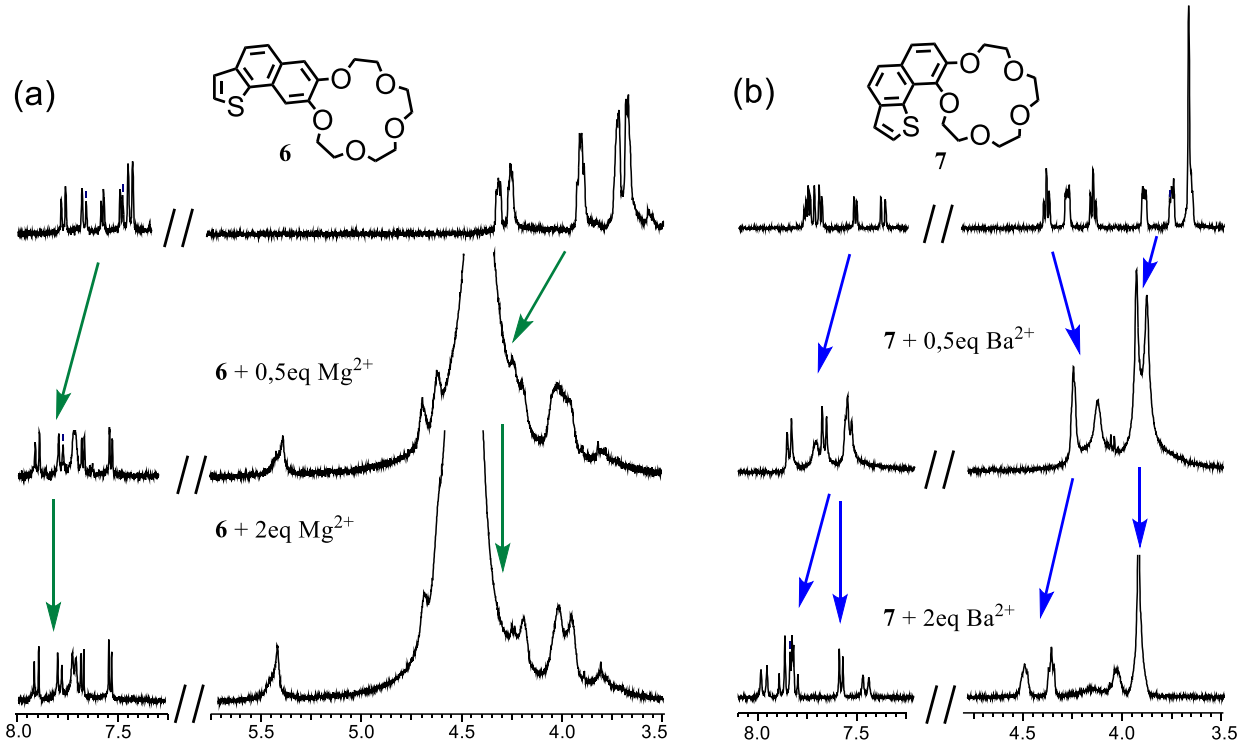

Figure S19. ^{1}H NMR spectral changes of (*a*) **4a** upon complexation with 0.5 equivalent of $Mg(ClO_4)_2$ and 2 equivalent of $Mg(ClO_4)_2$ and (*b*) of **4'a** upon complexation with 0.5 equivalent of $Ba(ClO_4)_2$ and 2 equivalent of $Ba(ClO_4)_2$.

UV-Vis titrations

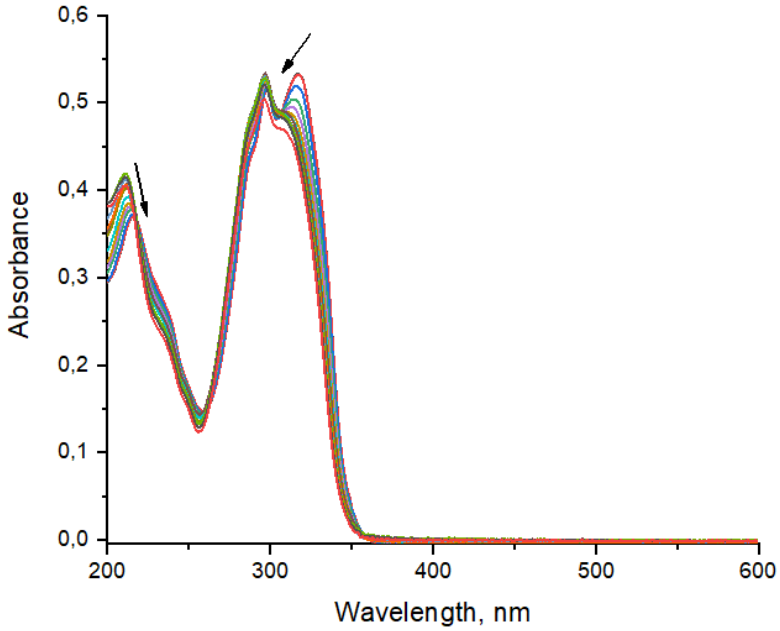

Figure S20. Electronic absorption spectra of complex **3a** in a MeCN solution at various concentrations of barium perchlorate. The initial concentration of **3a** $C=2\cdot10^{-5}$ mol·dm^{-3}, the concentration of salt varies in the range of $0 – 2\cdot10^{-4}$ mol·dm^{-3}.

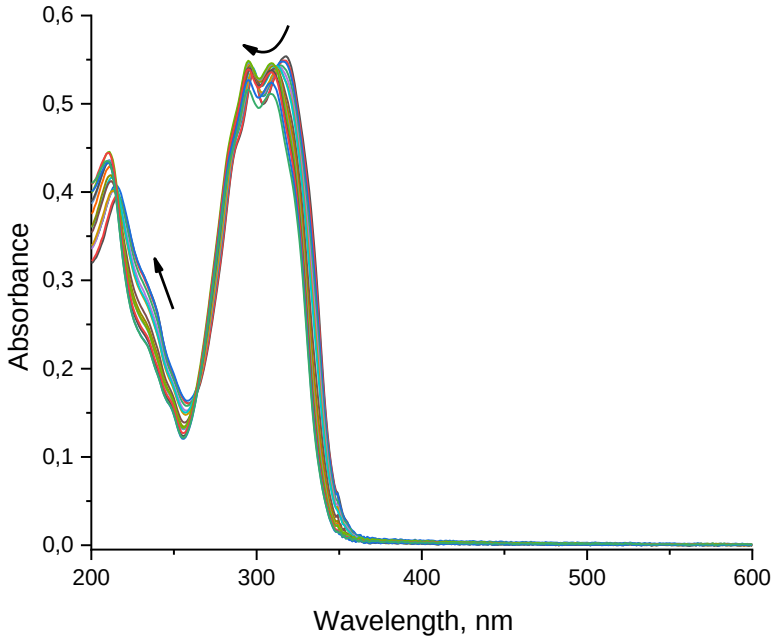

Figure S21. Electronic absorption spectra of complex **3a** in a MeCN solution at various concentrations of magnesium perchlorate. The initial concentration of **3a** C=2·10^{-5} mol·dm^{-3}, the concentration of salt varies in the range of 0 – 2·10^{-4} mol·dm^{-3}.

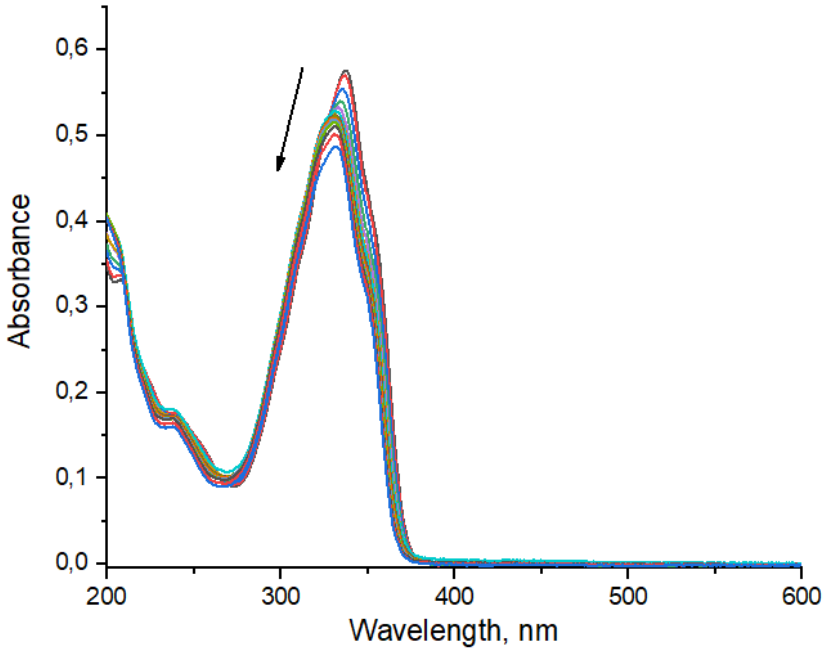

Figure S22. Electronic absorption spectra of complex **3b** in a MeCN solution at various concentrations of barium perchlorate. The initial concentration of **3b** C=2·10^{-5} mol·dm^{-3}, the concentration of salt varies in the range of 0 – 2·10^{-4} mol·dm^{-3}.

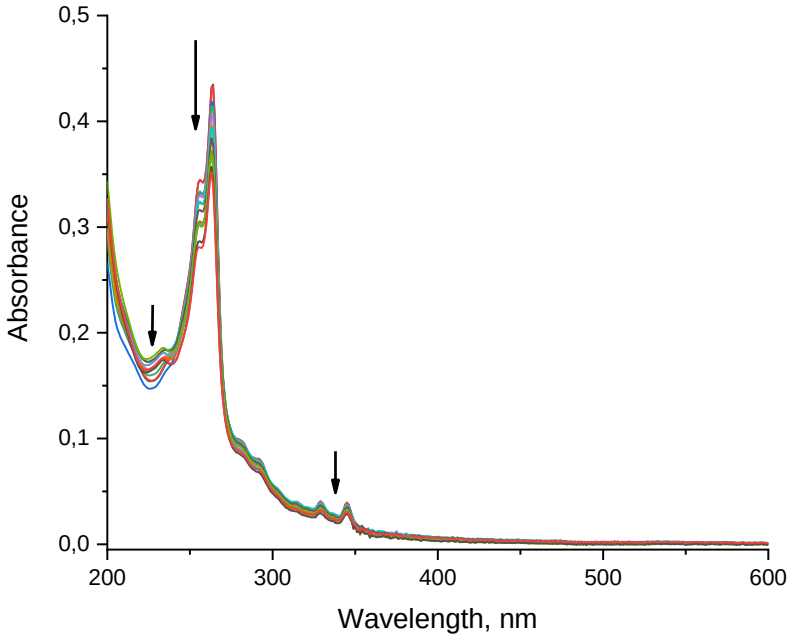

Figure S23. Electronic absorption spectra of complex **4a** in a MeCN solution at various concentrations of barium perchlorate. The initial concentration of **4a** C=2·10^{-5} mol·dm^{-3}, the concentration of salt varies in the range of 0 – 2·10^{-4} mol·dm^{-3}.

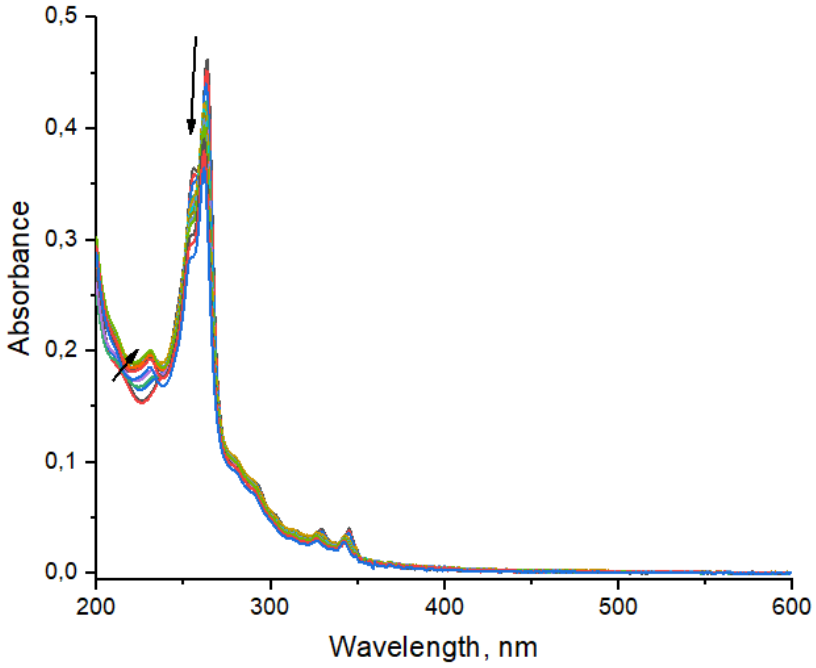

Figure S24. Electronic emission spectra of complex **4a** in a MeCN solution at various concentrations of magnesium perchlorate. The initial concentration of **4a** C=2·10^{-5} mol·dm^{-3}, the concentration of salt varies in the range of 0 – 2·10^{-4} mol·dm^{-3}.

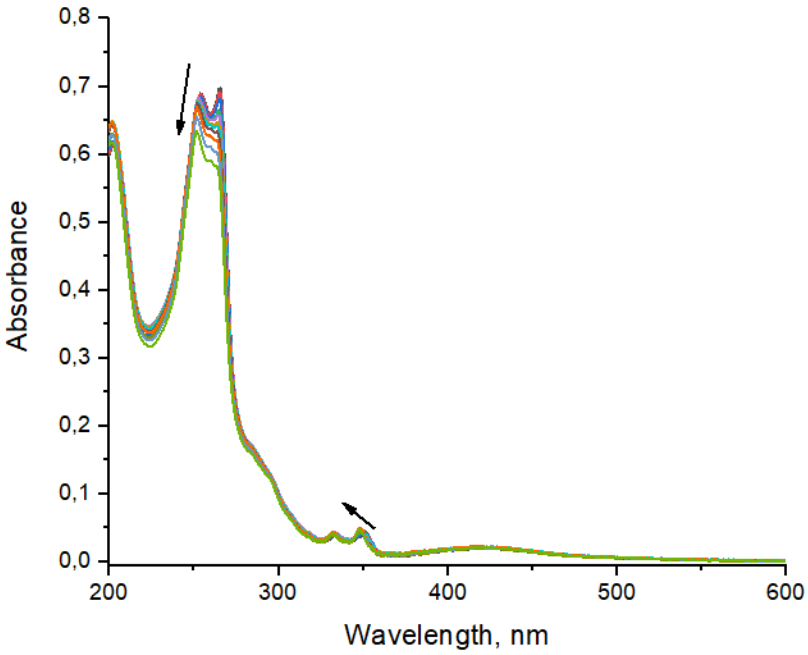

Figure S25. Electronic absorption spectra of complex **4'a** in a MeCN solution at various concentrations of barium perchlorate. The initial concentration of **4'a** C=2·10^{-5} mol·dm^{-3}, the concentration of salt varies in the range of 0 – 2·10^{-4} mol·dm^{-3}.

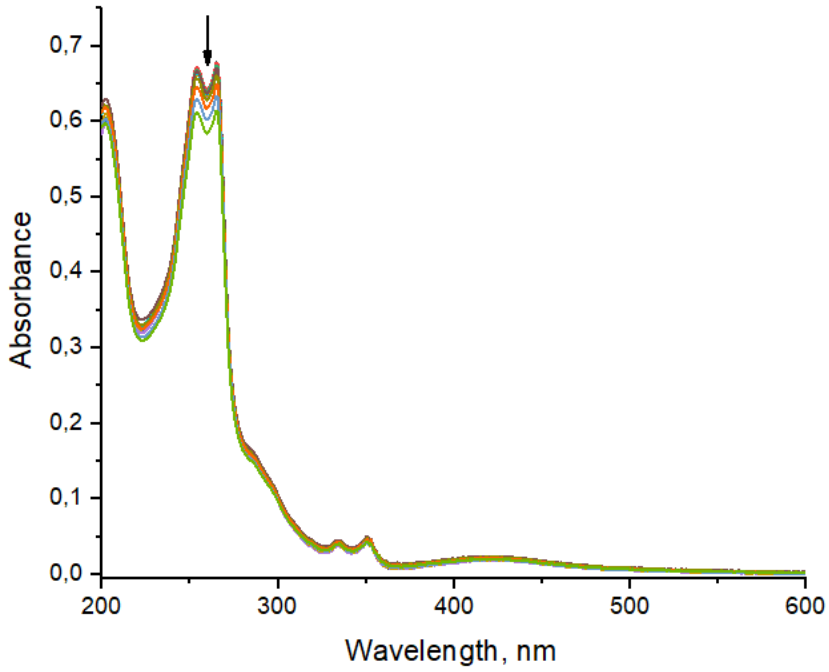

Figure S26. Electronic emission spectra of complex **4'a** in a MeCN solution at various concentrations of magnesium perchlorate. The initial concentration of **4'a** C=2·10^{-5} mol·dm^{-3}, the concentration of salt varies in the range of 0 – 2·10^{-4} mol·dm^{-3}.

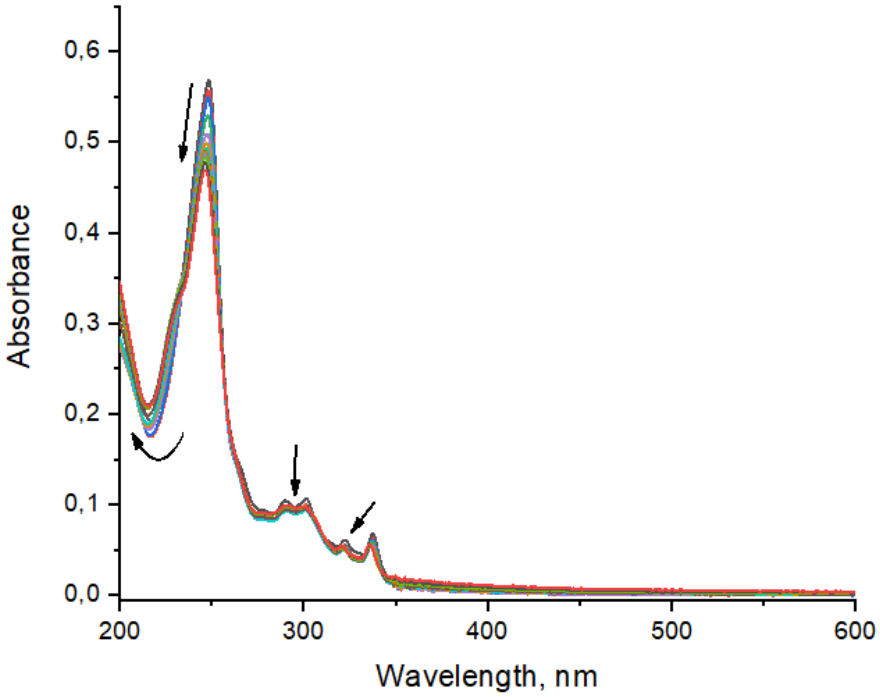

Figure S27. Electronic absorption spectra of complex **4b** in a MeCN solution at various concentrations of barium perchlorate. The initial concentration of **4b** C=2·10^{-5} mol·dm^{-3}, the concentration of salt varies in the range of 0 – 2·10^{-4} mol·dm^{-3}.

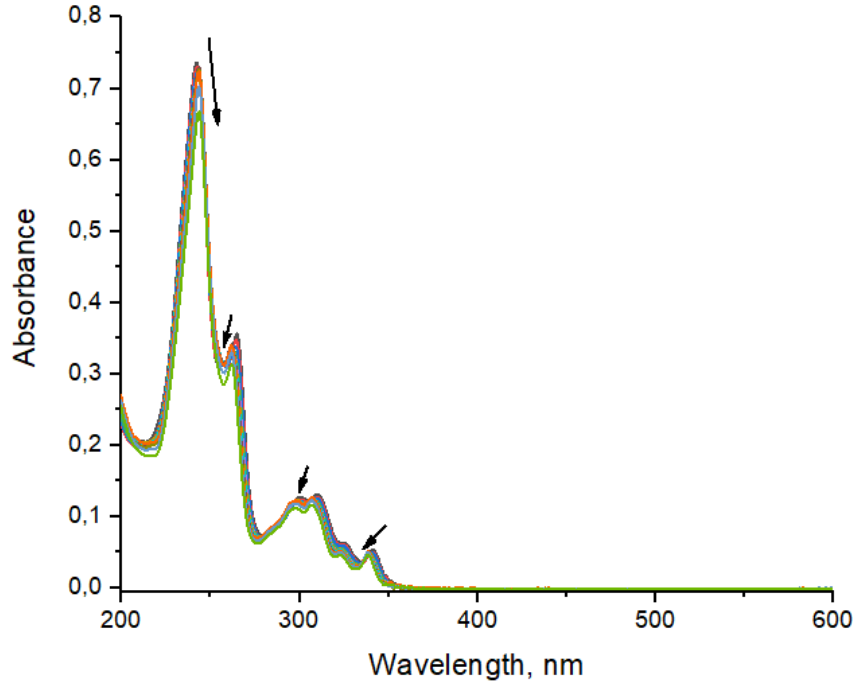

Figure S28. Electronic absorption spectra of complex **4'b** in a MeCN solution at various concentrations of barium perchlorate. The initial concentration of **4'b** C=2·10^{-5} mol·dm^{-3}, the concentration of salt varies in the range of 0 – 2·10^{-4} mol·dm^{-3}.

Electrochemistry

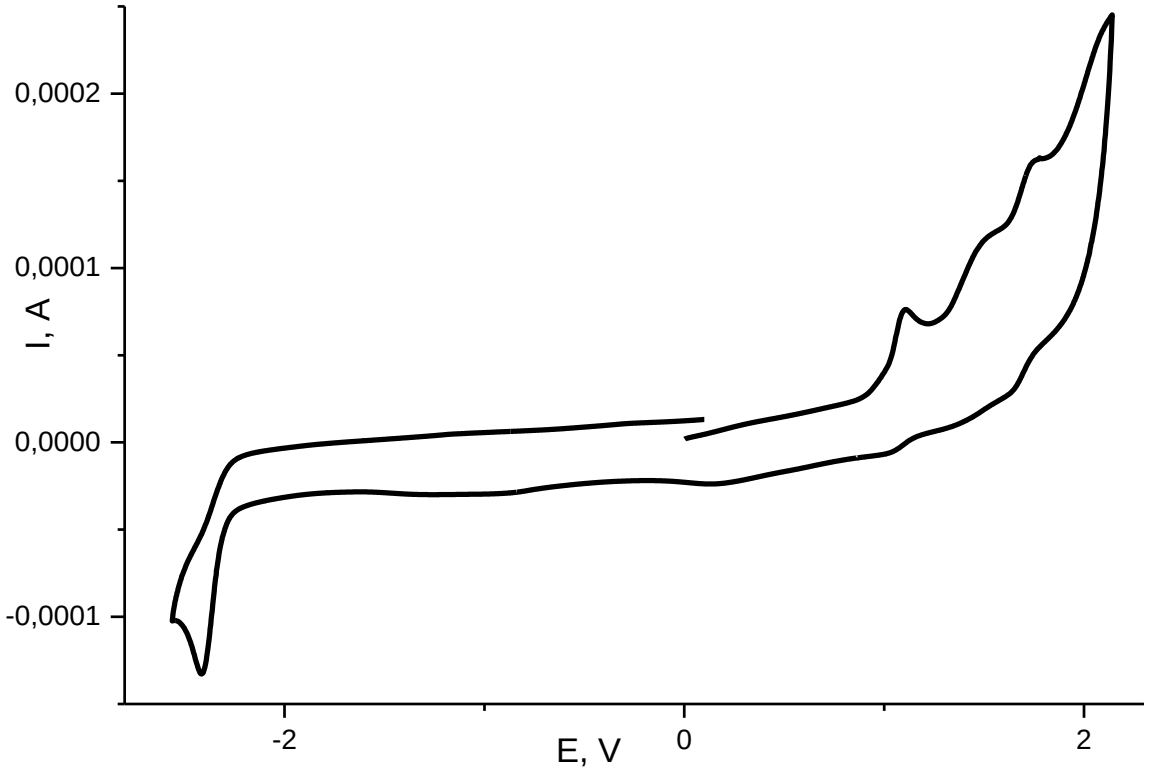

Figure S29. CVA of **3a** *vs* Ag/AgCl. (dcm, $C = 5 \cdot 10^{-4}$ M, supporting electrolyte NBu_4ClO_4, glassy carbon electrode, scan rate 200 mV s^{-1}).

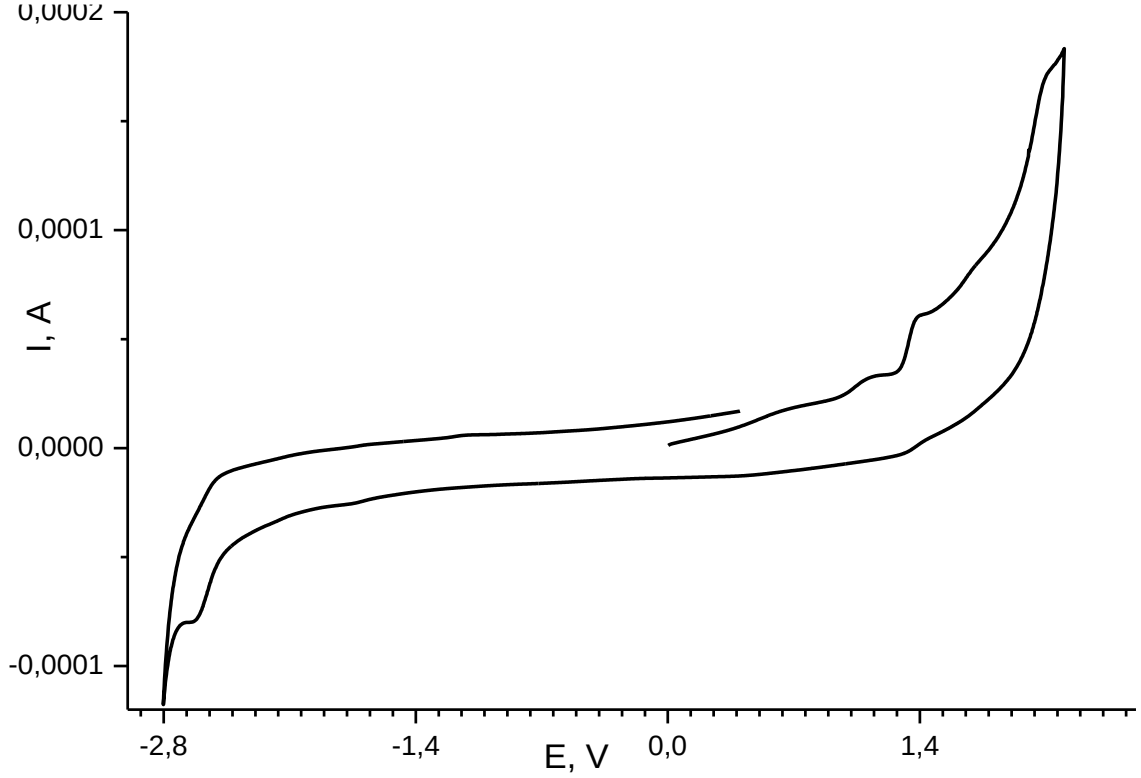

Figure S30. CVA of **4a** *vs* Ag/AgCl. (dcm, $C = 5 \cdot 10^{-4}$ M, supporting electrolyte NBu_4ClO_4, glassy carbon electrode, scan rate 200 mV/s).

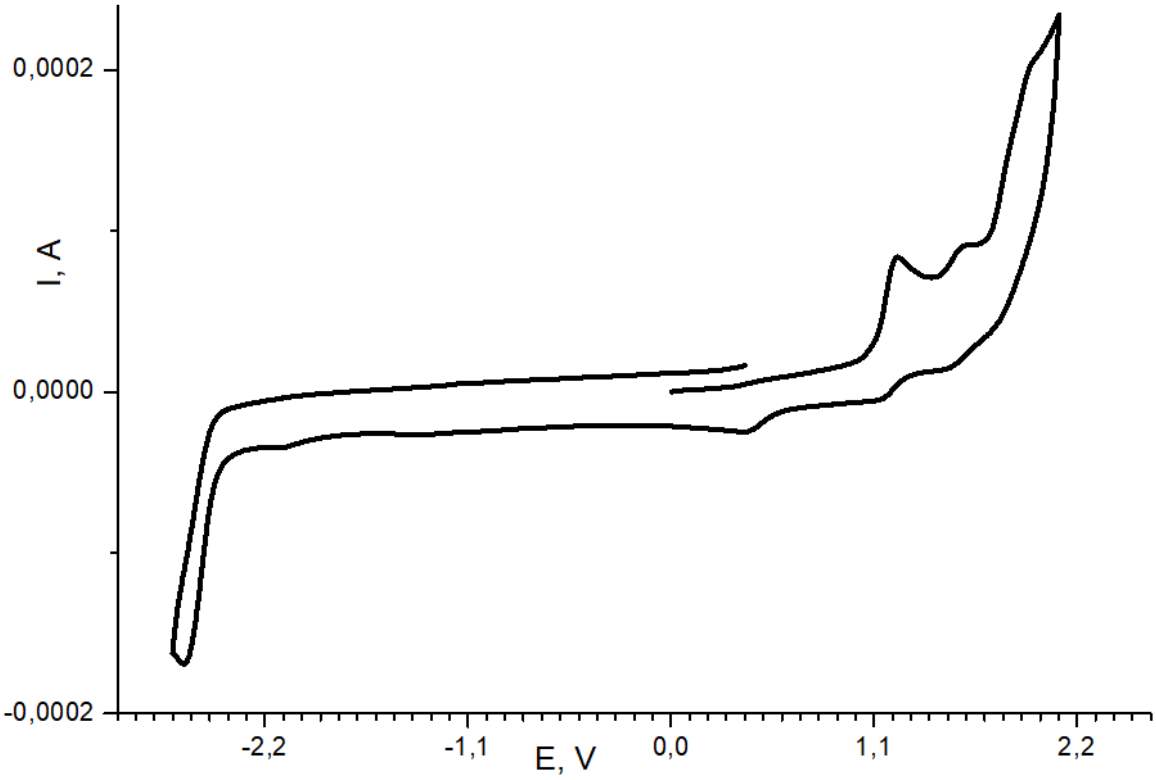

Figure S31. CVA of **4'a** *vs* Ag/AgCl. (dcm, $C = 5 \cdot 10^{-4}$ M, supporting electrolyte NBu_4ClO_4, glass carbon electrode, scan rate 200 mV/s).

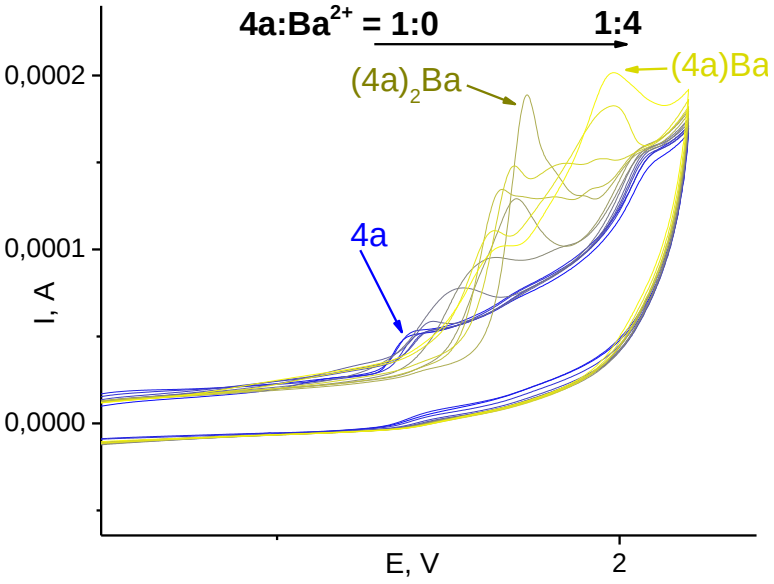

Figure S32. Changes in CVA of **4a** upon the addition of barium perchlorate

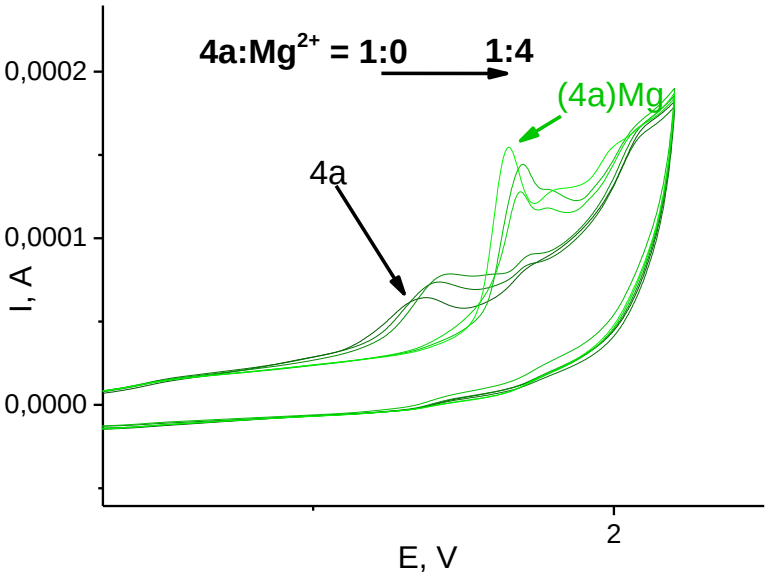

Figure S33. Changes in CVA of **4a** upon the addition of magnesium perchlorate

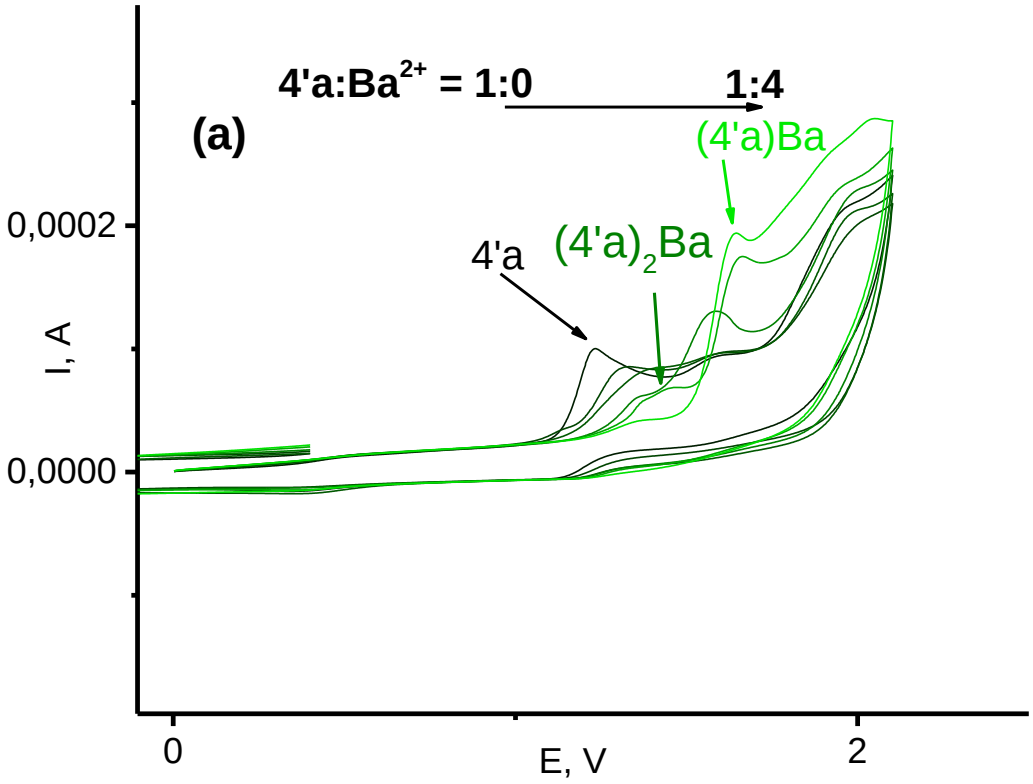

Figure S34. Changes in CVA of **4'a** upon the addition of barium perchlorate

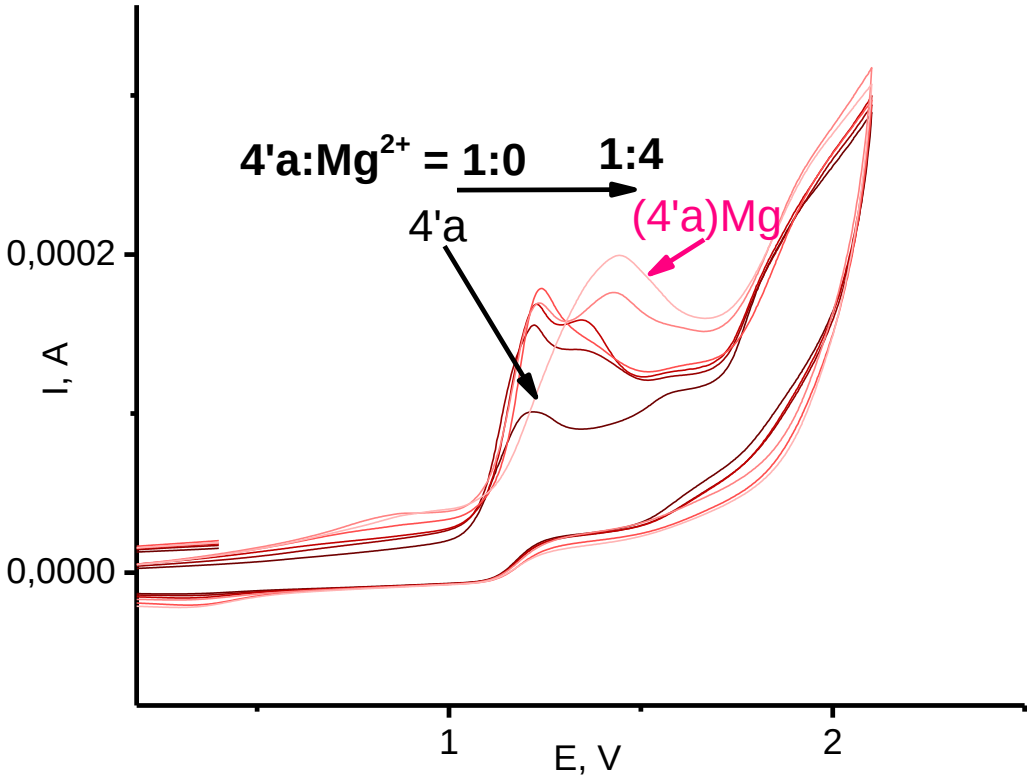

Figure S35. Changes in CVA of **4'a** upon the addition of magnesium perchlorate.

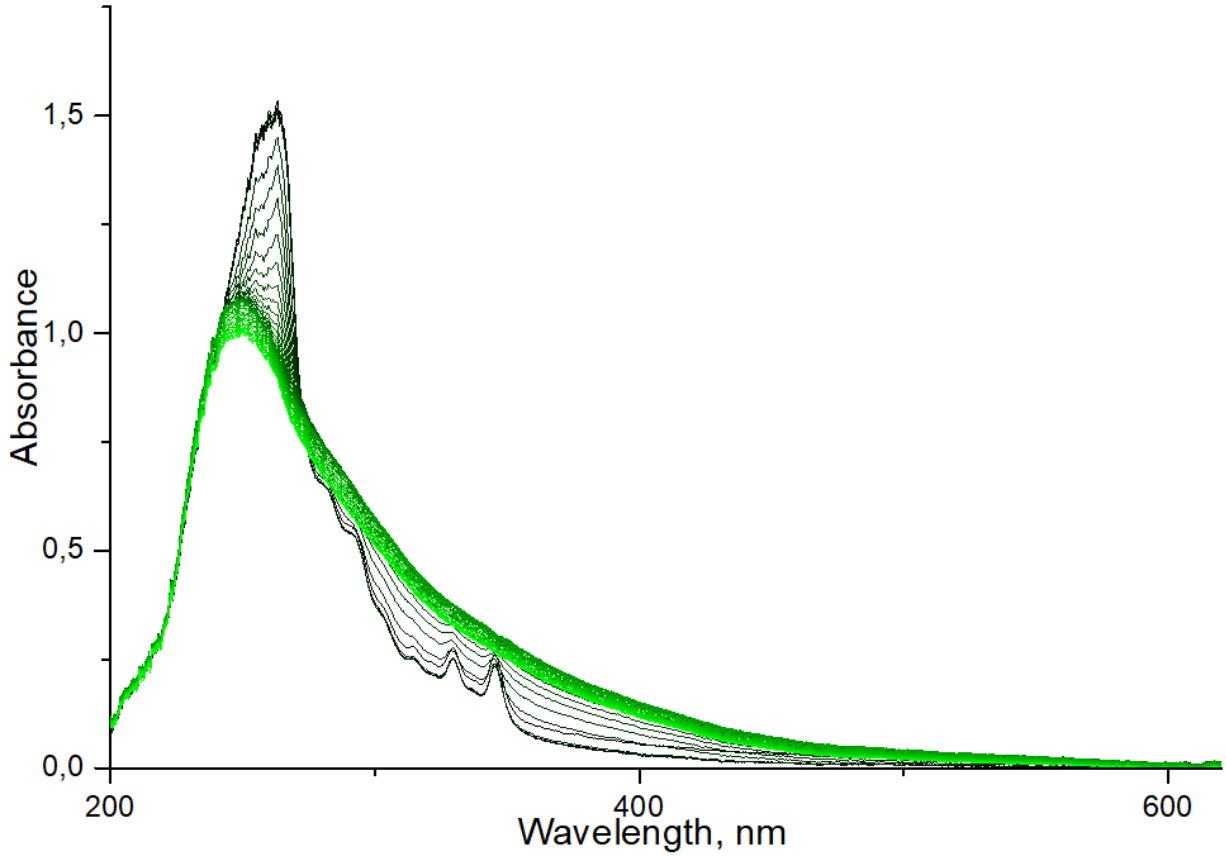

Figure S36. Changes in absorption spectrum of **4a** while applying potential of 1.4 V.

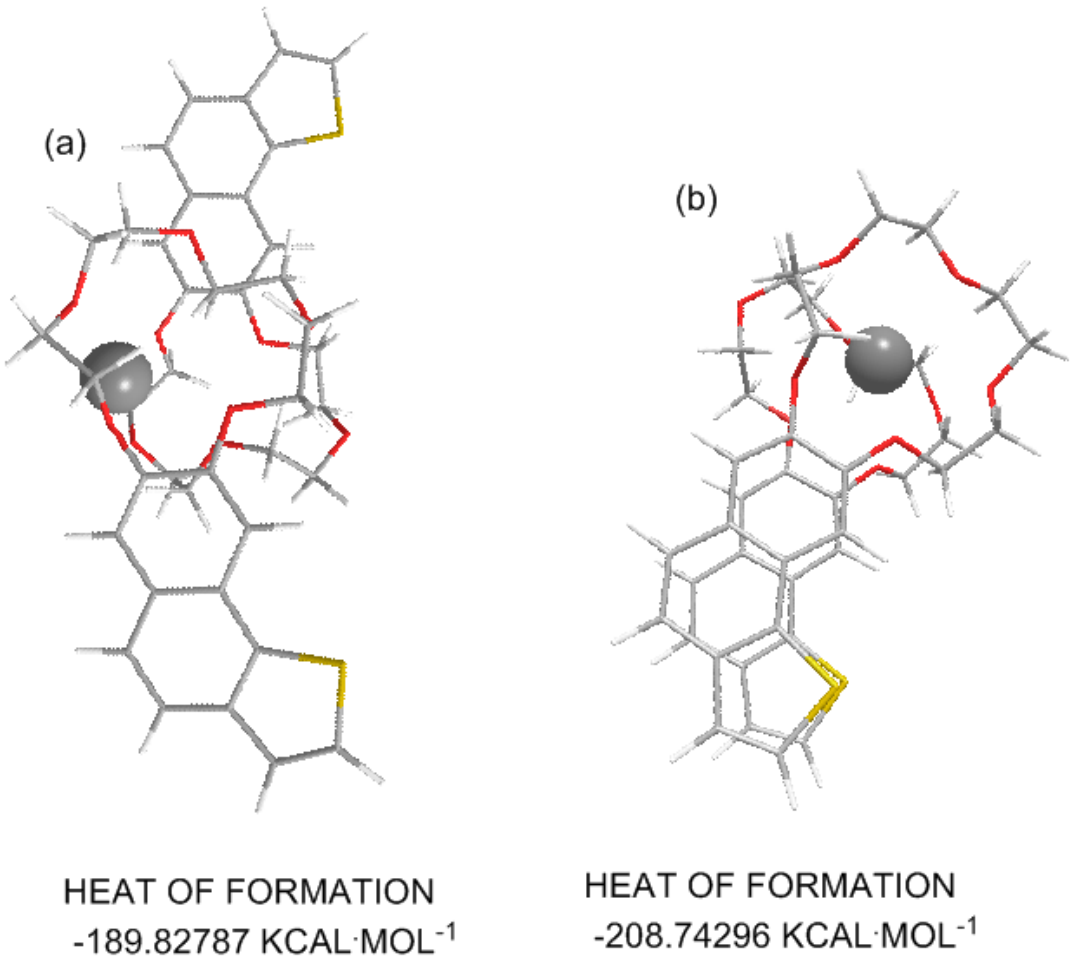

Figure S37. Optimized geometries of complex (**4a**)$_2$Ba in (*a*) *anti*- and (*b*) *syn*-configuration.

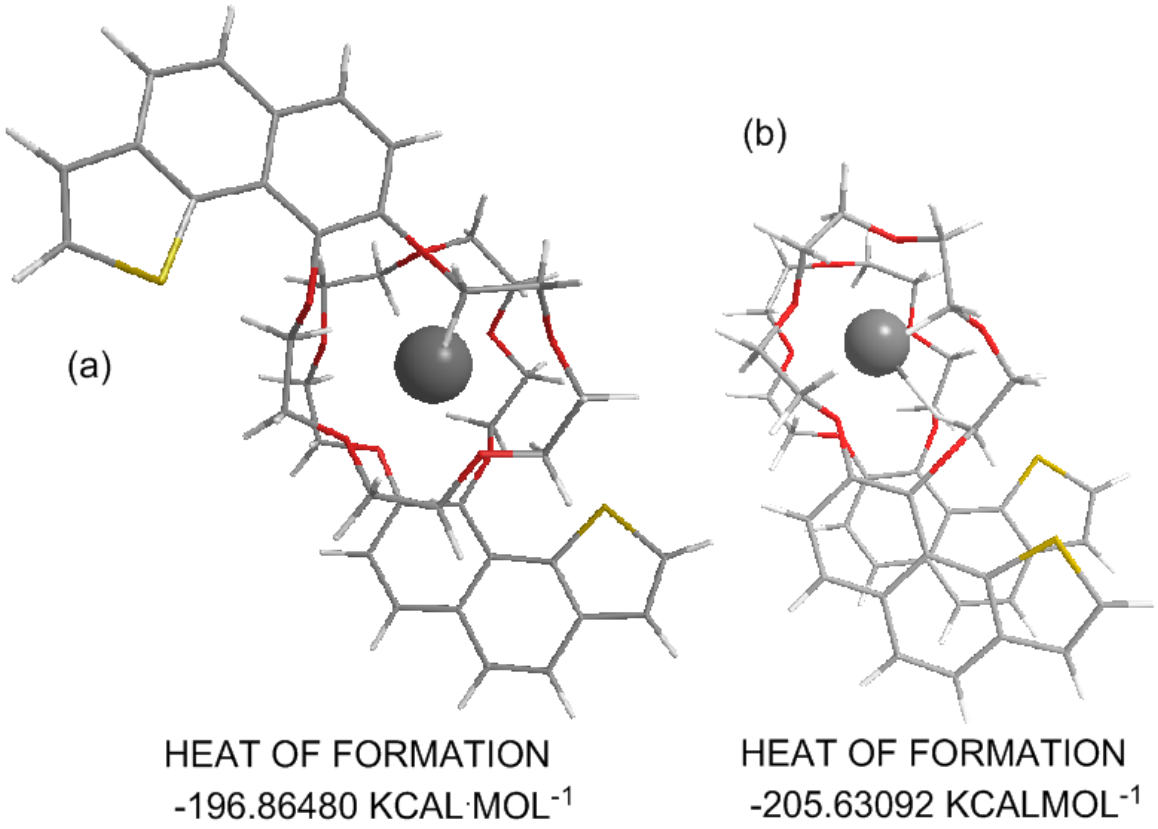

Figure S38. Optimized geometries of complex (**4'a**)$_2$·Ba in (*a*) *anti*- and (*b*) *syn*-configuration.

Table S1. Frontier orbitals and their energies (eV) of the cation radicals of **4a** and **4'a** as the results of UB3LYP/6-31+g(d) structure optimization.

	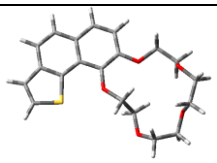 **4'a**				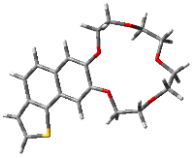 **4a**			
	A		B		A		B	
101	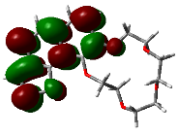	-4.46	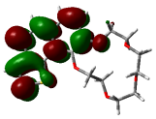	-4.23	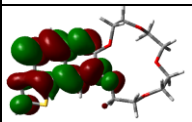	-4.61	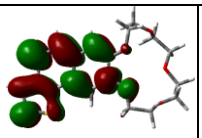	-4.23
100	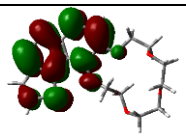	-5.22	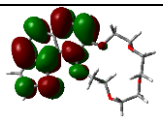	-4.74	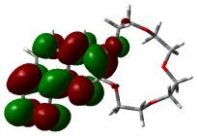	-5.02	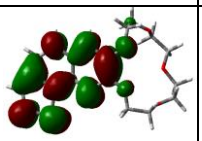	-4.70
99	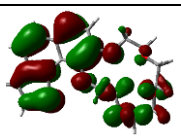	-9.30 SOMO	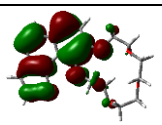	-7.77 LUMO	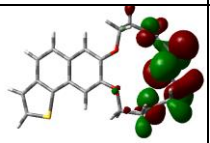	-9.21 SOMO	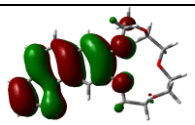	-8.03 LUMO
98	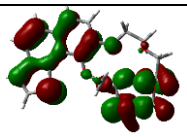	-9.46	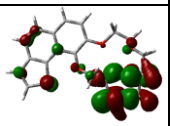	-9.41 HOMO	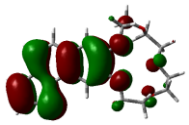	-9.49	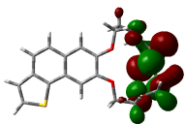	-9.21 HOMO
97	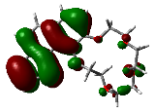	-9.67	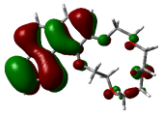	-9.60	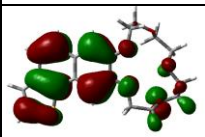	-9.57	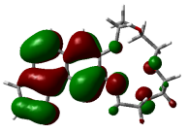	-9.47
96	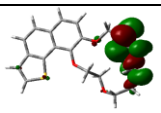	-9.96	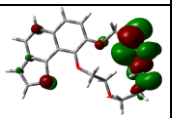	-9.95	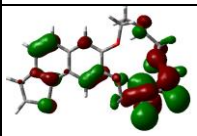	-9.66	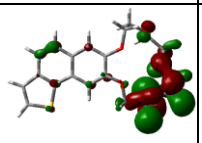	-9.65